DETECTION AND EXCLUSION OF FAULTY GNSS MEASUREMENTS: A PARAMETERIZED QUADRATIC PROGRAMMING APPROACH AND ITS INTEGRITY

by

Teng-Yao Yang

A Dissertation

Submitted to the Faculty of Purdue University

In Partial Fulfillment of the Requirements for the Degree of

Doctor of Philosophy

School of Aeronautics & Astronautics

West Lafayette, Indiana

May 2020

THE PURDUE UNIVERSITY GRADUATE SCHOOL
STATEMENT OF DISSERTATION APPROVAL

Dr. Dengfeng Sun, Chair

School of Aeronautics and Astronautics

Dr. Martin Corless

School of Aeronautics and Astronautics

Dr. James Garrison

School of Aeronautics and Astronautics

Dr. Jianghai Hu

School of Electrical and Computer Engineering

Dr. Inseok Hwang

School of Aeronautics and Astronautics

Approved by:

Dr. Gregory Blaisdell

Head of the School Graduate Program

To my parents and all the kind people.

ACKNOWLEDGMENTS

I would like to thank my advisor, Professor Dengfeng Sun, for giving me this opportunity to pursue this research. Under his guidance, I have continued to benefit from his comprehensive knowledge and skill as a mentor and a researcher. I will always be grateful for the wonderful experience.

I would like to express my gratitude to the other member in my defense and reading committee, Professor Martin Corless, Professor James Garrison, Professor Inseok Hwang, and Professor Jianghai Hu, for their constructive evaluation and criticism of this thesis.

I would like to thank Professor Arthur Frazho. for his inspirational lectures on mathematics.

I would like to thank Professor Shau-Shiun Jan and Dr. Shou-Ju Yeh, for sharing their data and making this research possible.

I would like to thank all the wonder people I met here in the Purdue University.

I thank Dr. Benjamin Claus, who has always been sincere and willing to help. In addition, it's always pleasant to work with the wonderful tools that he built himself.

In no particular order, I thank Dr. Yao-Cheng Lin, Dr. Chia-Chun Tang, Dr. Kuo-Nung Wang, Dr. Enyi Jan, Dr. Jou-Mei Chu, Dr. Yu-Chi Su, Dr. Jun Chen, and Dr. Boon Him Lim. I also thank Zherui Guo, Nesderin Kedir, Kody Kirk, Abi Komanduru, Harris Ho Soon Chye, Hsun Chao, Bang-Shiuh Chen, Jung-Ting Tsai,

and Philip Cho, for being wonderful friends for the past several years. I will alway cherish the memories we share together.

Last but not least, I would like to thank my parents. I would not accomplish anything without the love and the support they've been giving me.

TABLE OF CONTENTS

LIST OF TABLES

LIST OF FIGURES

ABSTRACT

Author: Yang, Teng-Yao Ph.D.
Institution: Purdue University
Degree Received: May 2020
Title: Detection and Exclusion of Faulty GNSS Measurements: A Parameterized Quadratic Programming Approach And Its Integrity
Committee Chair: Dengfeng Sun

This research investigates the detection and exclusion of faulty global navigation satellite system (GNSS) measurements using a parameterized quadratic programming formulation (PQP) approach. Furthermore, the PQP approach is integrated with the integrity risk and continuity risk bounds of the Chi-squared advanced receiver autonomous integrity monitoring (ARAIM). The integration allows for performance evaluation of the PQP approach in terms of accuracy, integrity, continuity, and availability, which is necessary for the PQP approach to be applied to the vertical navigation in the performance-based navigation (PBN). In the case of detection, the PQP approach can also be integrated with the vertical protection level and the associated lower and upper bounds derived for the solution separation ARAIM. While there are other computationally efficient and less computationally efficient fault detection and exclusion methods to detect and exclude faulty GNSS measurements, the strength of the PQP approach can summarized from two different perspectives. Firstly, the PQP approach belongs to the group of the computationally efficient methods, which makes the PQP approach more favorable when it comes to detect and exclude multiple simultaneous faulty GNSS measurements. Secondly, because of the integration of the PQP approach with the integrity risk and continuity risk bounds of the Chi-squared ARAIM, the PQP approach is among the first computationally efficient fault detection and exclusion methods to incorporate the concept of integrity, which lies in the foundation of PBN. Despite the PQP approach not being a practical integrity

monitoring method in its current form because of the combinatorial natural of the integrity risk bound calculation and the rather conservative integrity performance, further research can be pursued to improve the PQP approach. Any improvement on the integrity risk bound calculation for the Chi-squared ARAIM can readily be applied to the integrity risk bound calculation for the PQP approach. Also, the connection between the PQP approach and the support vector machines, the application of the extreme value theory to obtain a conservative tail probability may shed light upon the parameter tuning of the PQP approach, which in turn will result in tight integrity risk bound.

1. INTRODUCTION

With the advent of the Global Positioning System (GPS) for civilian use and the advancement of modern avionics, the navigation of aircraft over the continental US (CONUS) has been moving from the routes defined by ground navigation aids toward the more flexible routes that are less restricted by the ground navigation aids [1]. One of this trend is the concept of the performance-based navigation (PBN) [2]. Compared to the traditional navigation methods, PBN reduces the need to maintain sensor-specific procedures, routes, and the associated costs. PBN also abstains from the need for development of new sensor-specific operations. Furthermore, PBN allows for more efficient use of airspace, which in turn results in benefits including shorter traveling time and fuel-efficient routes. The three different types of flight routes that are shown in Figure 1.1, Figure 1.2, and Figure 1.3 [3] illustrate the benefits of use of PBN in civil aviation. The conventional NAVAID route in Figure 1.1 shows a conventional flight route which is defined by the conventional ground navigation aids. Such a conventional flight route is restricted by the locations of the ground navigation aids and thus it may be an indirect flight route and does not result in the most efficient use of the airspace. The area navigation (RNAV) routes form a class of flight routes defined in PBN. Figure 1.2 illustrates a RNAV route. In addition to the ground navigation aids, the use of the satellite-based navigation systems is taken into consideration when defining the RNAV routes. The restrictions resulted from the ground navigation are reduced with the use of satellite-based navigation systems. At the same time, the reliance on ground navigation aids is also reduced. The required navigation performance RNP routes belong to another kind of flight routes that are defined in PBN. In addition to the use of ground navigation aids and the satellite-based navigation systems, the navigation system performance monitoring and alerting capabilities on-board of aircraft are taken into consideration when defining the RNP

routes. Despite the use of satellite-based navigation systems reducing the restrictions imposed by ground navigation aids, it imposes restrictions itself. In other words, the performance of the satellite-based navigation systems depends on a number of factors which may change during aircraft operations. Without any on-board performance monitoring and alerting capabilities, the design of the RNAV routes are relatively conservative so that the aviation safety is not compromised. Once the on-board performance monitoring and alerting capabilities are considered, the RNP routes can be designed to gain further benefits without compromising aviation safety.

One of the important aspects of the PBN is the use of the global navigation satellite systems (GNSS) and the associated augmentation systems. The most common usages of GNSS in civil aviation involve the use of single constellation GNSS and the augmentation systems. An example is the use of GPS and the wide-area augmentation system (WAAS) to provide navigation over the CONUS. While single constellation GNSS and the augmentation systems are commonly used in PBN, the rapid development of the satellite navigation systems around the world is expected to improve GNSS performance and further benefit PBN through the use of multi-constellation GNSS together with the augmentation systems. At the same time, new challenges arise which have to be carefully studied and resolved before the benefits of multi-constellation GNSS can be exploited.

1.1 The Performance-Based Navigation Concept

The concept of the PBN can be described by its three major components, the navigation application, the navigation specification, and the navaid infrastructure. Among the components, the navigation application specifies the application in terms of the navigation specification. The navaid infrastructure refers to the navigation aids that support the application. The navigation specification is a set of requirements that should be fulfilled to support the navigation application. In the PBN, the navigation specification specifies the performance requirements defined in terms of four

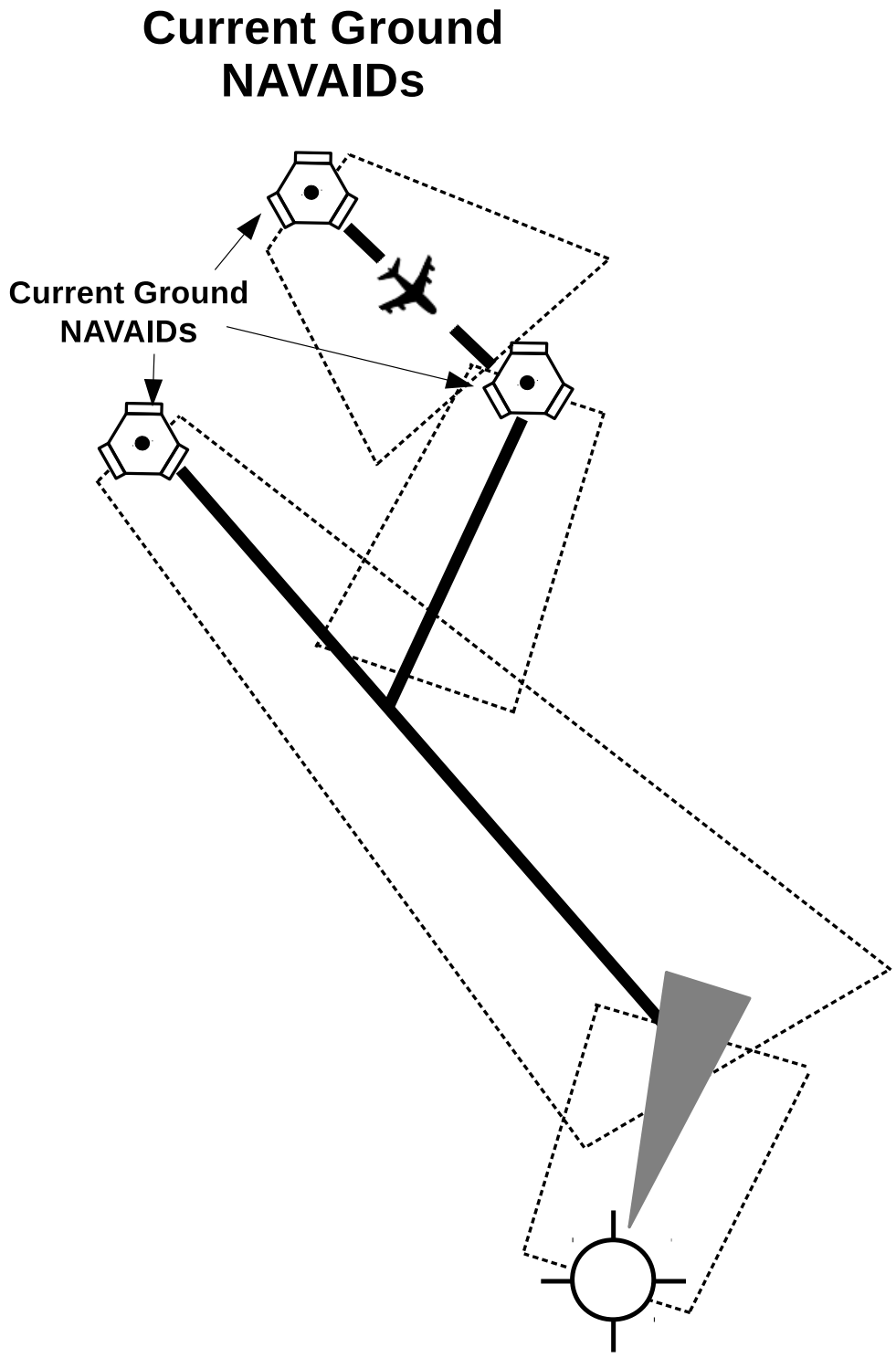

Figure 1.1. A conventional route.

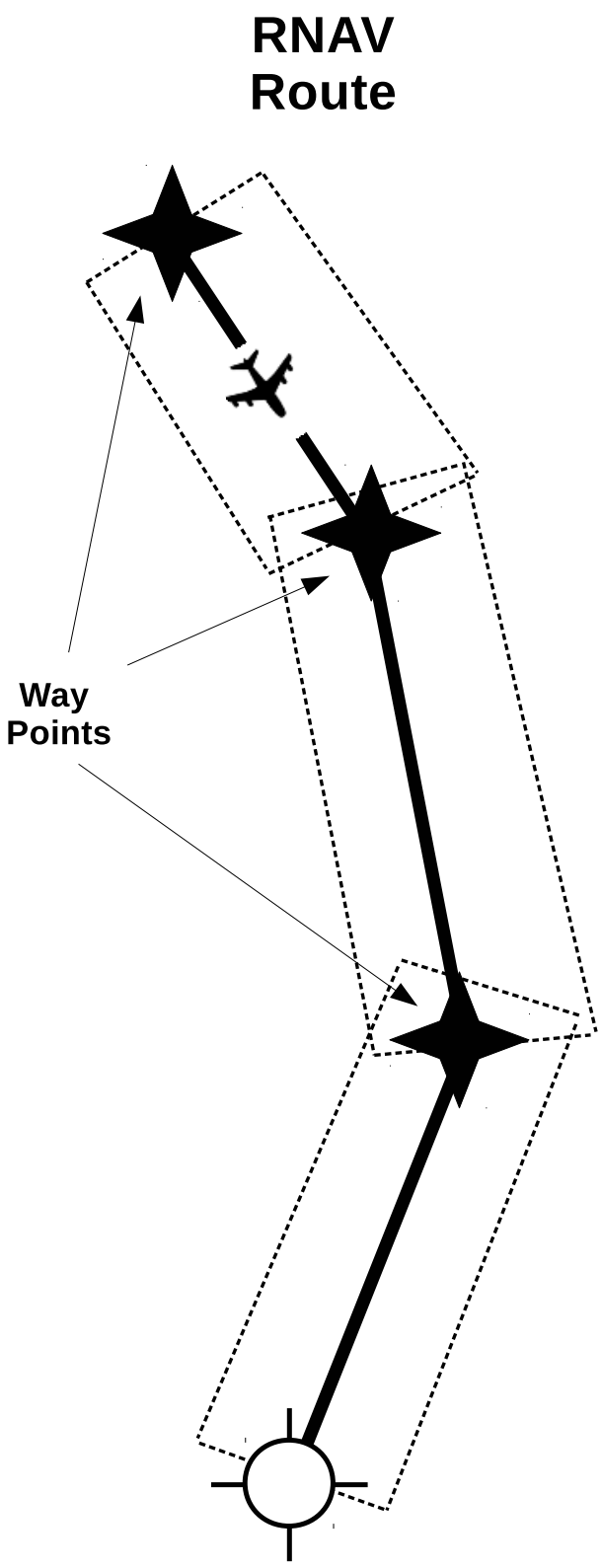

Figure 1.2. A RNAV route.

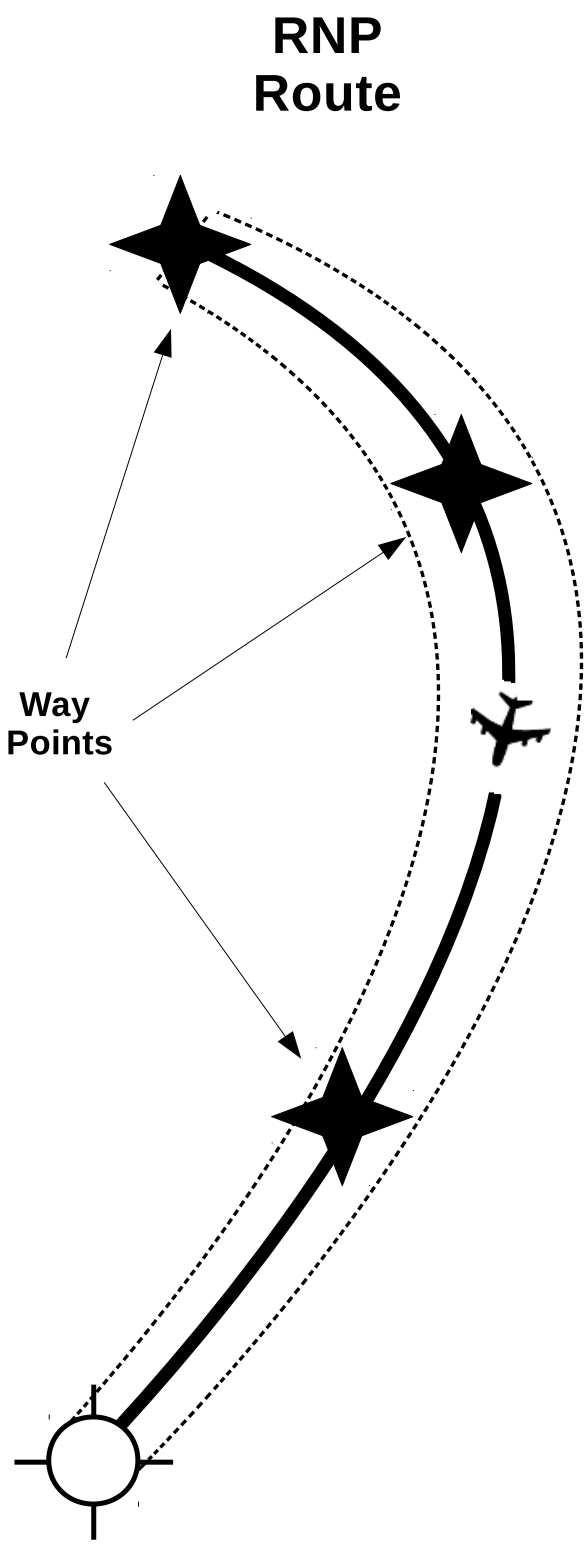

Figure 1.3. A RNP route.

parameters [4] accuracy, integrity, availability, continuity, and the required functionality to support the navigation application. The PBN navigation specification can be divided into two categories, the RNAV specification and the RNP specification. The RNAV specification specifies the requirements on the area navigation systems using the four parameters and thus incorporates the existing area navigation systems into the PBN. At the same time, the RNP specification is derived from the RNAV specification by the addition of the requirement of on-board performance monitoring and alerting capabilities.

1.1.1 Accuracy

Accuracy is a measure of position error, that is, the difference between the position estimated by navigation systems and the actual position of the user. When the position error is modeled as a random variable, the accuracy can be determined by the distribution function of the random variable. In general, it is the 95^{th} percentile of the position error. The horizontal accuracy and vertical accuracy can be similarly defined using the distribution functions of the horizontal and vertical position errors.

1.1.2 Integrity

Integrity is a measure of the trustworthiness of the position estimated generated by the navigation systems. The fulfillment of the integrity requirement can be determined by the calculation of integrity risk bound or protection level, both of which will be explained in detailed in the later chapters. For all PBN applications, the required upper limit of the associated integrity risk and alert limit are specified in the RNAV and RNP specifications. The integrity requirements are fulfilled if the calculated integrity risk bound does not exceed the required upper limit of integrity risk or if the calculated protection level does not exceed the required alert limit. Otherwise, the navigation systems must be able to provide timely warnings regard to the failure to fulfill the integrity requirement.

1.1.3 Continuity

Continuity refers to the ability of the navigation systems to provide the desired navigation functions without unscheduled interruptions, over the entire course of operation. Continuity can be characterized by continuity risk, which is the probability that a procedure will be interrupted by a loss of services. Similar to integrity, the fulfillment of the continuity requirement can be determined through the calculation of continuity risk bound. The continuity risk requirement is fulfilled if the calculated continuity risk bound does not exceed the required upper limit on continuity risk. Alternatively, the mathematical characterization of the continuity risk bound and the required upper limit on continuity can be incorporated into the integrity risk bound calculation. This way, the integrity risk bound calculation can be designed such that the continuity risk requirement is always fulfilled.

1.1.4 Availability

Availability is characterized by the probability that the requirements on accuracy, integrity, and continuity are all fulfilled at the beginning of the intended operation.

1.1.5 The Instrument Approaches

One of the most demanding flight phases is the approach. During the flight phase of approach, an aircraft is brought to the position that the pilot can initiate the landing procedures. The instrument approaches can be categorized into the non-precision approaches or the precision approaches. One of the main differences between the non-precision approaches and the precision approaches is that no vertical guidance is provided to the aircraft during the non-precision approaches while it is provided during the precision approaches [5]. Table 1.1 summaries the navigation specification for different types of instrument approaches. In Table 1.1, the lateral navigation (LNAV) belongs to the non-precision approaches, while the lateral nav-

Table 1.1. The NAS RNP

Typical Operation	Horizontal Accuracy (95%)	Vertical Accuracy (95%)	Integrity	Continuity	Horizontal Alert Limit (HAL)	Vertical Alert Limit (VAL)	Availability	Time to Alert
LNAV (NPA)	200m	NA	$1-10^{-7}$/hr	$1-10^{-4}$/hr to $1-10^{-8}$/hr	1852m	NA	.99 to .99999	10s
LNAV/ VNAV	200m	20m	$1-2\times10^{-7}$ /approach	$1-8\times10^{-6}$ / 15s	566m	50m	.99 to .999	10s
LPV	16m	20m	$1-2\times10^{-7}$ /approach	$1-8\times10^{-6}$ / 15s	40m	50m	.99 to .999	10s
APV-I	16m	20m	$1-2\times10^{-7}$ /approach	$1-8\times10^{-6}$ / 10s	40m	50m	.99 to .999	10s
APV-II	16m	8m	$1-2\times10^{-7}$ /approach	$1-8\times10^{-6}$ / 15s	40m	20m	.99 to .999	6s
CAT-I/ GLS	16m	6m to /4m	$1-2\times10^{-7}$ /approach	$1-8\times10^{-6}$ / 15s	40m	12m to /10m	.99 to .99999	6s
CAT-II and/ CAT-IIIa	6.9m	2.0	$1-2\times10^{-9}$/15s	$1-4\times10^{-6}$ / 15s	17.3m	5.3m	.99 to .99999	1s

igation/vertical navigation (LNAV/VNAV), the localizer performance with vertical guidance (LPV), the approach with vertical guidance-I (APV-I), the approach with vertical guidance-II (APV-II), the category-I (CAT-I) precision approach, the ground based augmentation system landing system (GLS), the category-II (CAT-II) precision approach, and the category-IIIa (CAT-IIIa) precision approach all belong to the precision approaches. This can be seen by noting that there's no requirement on the vertical accuracy for LNAV. Another remark to mention is that the navigation specification for each of the instrument approaches in Table 1.1 belongs to the RNP specification, since there are requirements on the integrity and the time to alert for each approach, and since such requirements are closely related to the on-board performance monitoring and alerting capabilities.

Among the most commonly used navigation systems during approaches are the instrument landing systems [6]. The instrument landing systems are comprised of four components, including a localizer, a glide slope, marker beacons, and approach lights. The localizer provides the horizontal guidance and the glide slope provides the vertical guidance, while the marker beacons furnish the distance information and the approach lights signal the transition from instrument to visual flight. The instrument landing systems are capable of providing the (CAT-I) precision approach,

the (CAT-II) precision approach, and the (CAT-III) precision approach. The need of an instrument landing system in an airport to provide the three categories of precision approaches, however, motivates the researches on using GNSS and the augmentation systems to provide the three categories of precision approaches

1.2 The Global Navigation Satellite Systems

The term global navigation satellite system (GNSS) refers to any of the satellite navigation systems providing positioning, navigation, and time (PNT) services. Currently, GNSS include the the Global Positioning System (GPS) of the United States [7], the Beidou Navigation Satellite System (BDS) of the People's Republic of China [8], the Galileo of the European Union [9], and the Global Navigation Satellite System (GLONASS) of the Russian Federation [10] that provide global coverage. In addition, GNSS include the Indian Regional Navigation Satellite System (IRNSS)/Navigation Indian Constellation (NavIC) of the Republic of India and the Quasi-Zenith Satellite System (QZSS) of Japan that provide regional coverage [11]. From the PBN perspective, GNSS provide new options for navigation infrastructure. In order for the PBN to benefit from GNSS, it is crucial that GNSS should be able to fulfill the performance requirements specified in the navigation specification. However, GNSS alone are not sufficient to fulfill the integrity requirements of the RNP specification, which requires the on-board performance monitoring and alerting capabilities. Augmentation systems are consequently proposed and developed. Depending on implementation, augmentation systems can be categorized into the Satellite-Based Augmentation Systems (SBAS) [12], the Ground-Based Augmentation Systems (GBAS) [13], and the Aircraft-Based Augmentation Systems (ABAS) [14].

1.2.1 Satellite-Based Augmentation Systems

In general, a SBAS is comprised of a network of ground reference stations, central data processing stations, and geostationary satellites. The SBAS augment GNSS by

providing differential corrections, integrity monitoring service, and additional ranging signals [12]. The ground reference stations are located at precisely known locations and are able to monitor anomalies, which are also called faults, by inspecting the received GNSS measurements. From the measurements received at the ground reference stations, the center data processing stations are able to generate vector corrections, which are then uploaded to the geostationary satellites and then broadcast to the users that are within its coverage. In addition, the signals broadcast from the geostationary satellites also serve as range measurements for the users inside the coverage. With the wide area augmentation system (WAAS) [15] developed by the Federal Aviation Administration of the Unite States, the GPS can be used to provide a type of instrument approach, which is very similar to the (CAT-I) precision approach and is called the localizer performance with vertical guidance approach, with decision height down to 200 ft (LPV-200) [16].

1.2.2 Operational and Developing Satellite-Based Augmentation Systems

Currently, the operational and developing SBAS include the wide area augmentation system (WAAS) of the United States, the multi-function satellite augmentation system (MSAS) of Japan [17], the European geostationary navigation overlay service (EGNOS) [18] of the the European Union, the GPS aided GEO augmented navigation (GAGAN) of the Republic of India [19], the system of differential corrections and monitoring (SDCM) of the Russian Federation [20], the Beidou satellite-based augmentation system (BDSBAS) of the People's Republic of China [21], and the Korean augmentation satellite system (KASS) of the Republic of Korea [22].

1.2.3 Ground-Based Augmentation Systems

Similar to the SBAS, a GBAS is comprised of multiple reference receivers and antennas, all of which are located at precisely known locations whose observations are used by a master control processor to generate corrections and to monitor the

integrity of GNSS [13]. Unlike the SBAS that broadcast the corrections through the geostationary satellites and therefore have wide coverage, the GBAS broadcast the corrections through the very high frequency (VHF) data transmitters and antennas and thus have local coverage. Consequently, the GBAS focus to serve particular locations, for example, airports. Like the instrument landing systems, the GBAS are able to provide all three categories of precision approaches, including the (CAT-I) precision approach, the (CAT-II) precision approach, and the (CAT-III) precision approach. As in 2017, the Newark Liberty International Airport (EWR) and the Houston George Bush Intercontinental Airport (IAH) are the two airports in the United States that have obtained operational GBAS approved for public use [13].

1.2.4 Aircraft-Based Augmentation System

While the SBAS and GBAS are able to provide precision approaches, respectively, down to the CAT-I and CAT-III precision approaches, they require expensive ground and/or space infrastructures. Unlike the SBAS and GBAS, the ABAS rely mostly on aircraft onboard equipment. One of the most commonly used ABAS is the receiver autonomous integrity monitoring (RAIM) [23, 24]. The RAIM uses redundant GNSS measurements to performance consistent check and detect the existence of faulty GNSS measurements. For a single constellation GNSS, at least four GNSS measurements are required to estimate the three components of the user position vector and the receiver clock bias. Consequently, at least five GNSS measurements are required to provide the necessary redundancy to use the RAIM in the context of single constellation GNSS.

1.2.5 Multi-Constellation Global Navigation Satellite Systems

One of the earliest studies regarding to multi-constellation GNSS is related to the integrated use of the GPS and GLONASS in civil aviation [25]. It is reported in the study that the integrated use of the GPS and GLONASS results in better satellite

geometries and accuracy. The integrity supported by the RAIM also improved. It is also reported in [26] that the use of multi-constellation GNSS may include the global coverage of vertical guidance of aircraft, which not only provides more efficient use of the airspace but also reduces the development and maintenance cost of the space and ground infrasturcture.

1.2.6 Fault Detection and Exclusion of Faulty Measurements

GNSS measurements are vulnerable to interference, both unintentional and intentional [27]. For example, interference can be caused by the multi-path effect [28], the ionosphere scintillation [29], and the spoofing attacks [30]. Under the influence of interference, the noise imposed on a GNSS measurement my deviate greatly from the nominal measurement error model. In this case, the measurement is considered as a faulty measurement. Faulty measurements, if any, may degrade significantly the performance of GNSS. In this regard, it is important to be able to detect and exclude faulty GNSS measurements. Despite that the RAIM supports the on-board integrity monitoring capability, which is required by the RNP navigation specification, by detecting the presence of faulty measurements, the problems that are caused by the faulty measurements are not completely solved. Knowing the existence of faulty measurements makes it possible to avoid the use of GNSS in safety-critical aviation applications and thus the potential dangers, it suggests the need to recover, or at least remove, those faulty measurements at the same time. Otherwise, alternative navigation systems available and can be used in place of the GNSS. Therefore, the crux of the problem is that unless the performance can be brought back to the nominal state after the detection of faulty measurements, by either exclusion or restoration, it will be difficult to fully exploit the benefits GNSS have to offer. This problem has more effect in the multi-constellation GNSS, since the probability that one or more measurements received are faulty is increased in the multi-constellation GNSS. Recovery

from or exclusion of the faulty measurements, and then bring the GNSS performance back to nominal state is of great importance.

1.3 Sparse Approximation of Signals

A branch of research in signal processing that is seemingly unrelated to the PBN and GNSS is the sparse approximations of signals. To be more precise, researches on the sparse approximate solutions to underdetermined linear systems [31] are closely related to the detection and exclusion of the faulty GNSS measurements. Since an underdetermined linear system may have more than a single unique solution, different types of methods are proposed for this task. For instance, regularization methods can be leveraged to find solutions to underdetermined linear systems [32]. In signal processing, a sparse approximation of a signal is a linear combination of a set of basis signals such that most of the coefficients of the linear combination vanish. Finding a sparse approximation of a signal is closely related to finding a sparse and appropriate solution to a system of underdetermined linear system [33],

$$\min_{\mathbf{z}\in\mathbb{R}^n} \|\mathbf{z}\|_0, \tag{1.1}$$

such that

$$\mathbf{y} = \mathbf{A}\mathbf{z}. \tag{1.2}$$

given $\mathbf{A} \in \mathbb{R}^{m\times n}$, $m, n \in \mathbb{N}$, and $m < n$.

1.3.1 Greedy Algorithms

Finding a sparse approximation of a signal amounts to solving for a solution to (1.1). One common type of strategies employed involves the use of the greedy algorithms [34], which iteratively construct a new and locally optimized approximation using a new basis signal and the most current approximation until the newly

constructed approximation is good enough in some criterion. Some of the most commonly used greedy algorithms include the various variants of the pursuit algorithms, including the matching pursuits [35] and the basis pursuit [36]. In particular, sufficient conditions for exact recovery of the signals using the orthogonal matching pursuit have been established in [37].

1.3.2 Convex Relaxation Algorithms

In addition to the greedy algorithms, (1.1) can also be solved exactly by exhaustive search. However (1.1) has been proved to be of NP-hardness [38], and can be solved exactly only by exhaustive search. Approaching the sparse approximate solution to (1.1) by exhaustive search is therefore not practical. One method to overcome this difficulty is to replace the objective function of the l_0 minimization problem by the l_1-norm of the vector of coefficients [39]. The resulting l_1 minimization problem is convex, and it can be reformulated into a linear programming (LP) problem or a quadratic programming (QP) problem and then be efficiently solved.

1.3.3 Exactly Recovery through the l_1-minimization and the Restricted Isometry Property

One question that naturally follows the convex relaxation algorithms is that, can a signal be perfectly reconstructed by the solution to the l_1-minimization problem? For noiseless measurements, the question can be answered by the concept of the null space property [40] of matrices. For a matrix $\mathbf{M} \in \mathbb{R}^{m \times n}$, $\mathbf{M}$ satisfies the null space property relative to a subset of the indices $\{1, 2, \ldots, n\}$, denoted by S, if

$$\|\mathbf{v}_S\|_1 < \|\mathbf{v}_{\overline{S}}\|_1, \tag{1.3}$$

for all $\mathbf{v} \in \ker \mathbf{M} \setminus \mathbf{v}_\Theta$, where $\mathbf{v}_S$ is the vector formed using the components of the vector $\mathbf{v}$ that correspond to the indices in S and $\mathbf{v}_{\overline{S}}$ is the vector formed using the

components of that correspond to the indices not in S, $\ker \mathbf{M}$ is the kernel of the matrix $\mathbf{M}$, and $\mathbf{v}_\Theta$ is the zero vector of $\mathbb{R}^n$ [41]. Given any $\mathbf{x} \in \mathbb{R}^n$ such that the support of $\mathbf{x}$ has cardinal number s and if

$$\mathbf{y} = \mathbf{M}\mathbf{x}, \tag{1.4}$$

then $\mathbf{x}$ is the unique solution to

$$\min_{\mathbf{x}\in\mathbb{R}^n} \|\mathbf{x}\|_1, \tag{1.5}$$

such that

$$\mathbf{y} = \mathbf{M}\mathbf{x}, \tag{1.6}$$

if and only if $\mathbf{M}$ satisfies the null space property relative to all the subsets of the indices $\{1, 2, \ldots, n\}$ that have cardinal number s. Two remarks are made here. Firstly, checking whether or not a matrix $\mathbf{M}$ satisfies the null space property relative to a subset of indices S can be difficult since it is necessary to wade through all the nontrivial vector that are in the kernel of $\mathbf{M}$ and all the appropriate subsets of indices. Secondly, if a the necessary and sufficient conditions can be verified to be true, then the solution to (1.5) reconstructs $\mathbf{x}$ from only the noiseless measurements. Unfortunately, measurements are almost always corrupted in practical applications.

1.4 Issues Addressed and Dissertation Organization

This dissertation investigates the application of sparse approximations of signals to the detection and exclusion of faulty GNSS measurements. To be more specific, the detection and exclusion are modeled as a l_0-minimization problem that takes the form of (1.1). Convex relaxation is then adopted and the l_0-minimization problem is turned into a l_1-minimization problem of the form of (1.5). The goal of the convex relaxation is to make the l_0-minimization problem tractable for real-time detection and exclusion

of faulty GNSS measurements in aviation application, and accompanying the convex relaxation are some important issues that are addressed in this dissertation.

1.4.1 The Parameterized Quadratic Programming Formulation of the l_1-minimization Problem

Since measurements in practical applications are corrupted by noise in general, the variant of the l_1-minimization problem described by (1.5) is considered

$$\min_{\mathbf{z}\in\mathbb{R}^n} \|\mathbf{z}\|_1, \tag{1.7}$$

such that

$$\|\mathbf{y} - \mathbf{A}\mathbf{z}\|_2 \leq \epsilon. \tag{1.8}$$

In (1.7), ϵ is a positive constant that is accommodated to reflect the fact the measurements are corrupted by noise. Various methods to solve (1.7) are proposed and studied extensively [42]. For example, (1.7) can be reformulated into a linear programming (LP) problem [43]. The formulation adopted is the parameterized quadratic programming problem proposed in [36]. The fault detection and exclusion algorithm depends not only on the approximations of the sparse signals but also on the RAIM. The parameterized quadratic programming allows for the integration of the approximations of the sparse signals and the RAIM, which in turn lead to the characterization of the continuity risk and integrity risk bounds. Therefore, it is possible to evaluate the performance of the proposed detection and exclusion algorithm when it is intended to be used in PBN applications. The problem of detection and exclusion of faulty GNSS measurements is stated in Chapter 2, together with the description of the RAIM for fault detection. The l_0-optimization, the l_1-optimization, and the parameterized quadratic formulation are presented in Chapter 3, in which the deriva-

tion of the integrity risk bound for the parameterized quadratic formulation is also shown.

1.4.2 Two Parameterized Tuning Methods

Parameter tuning plays a crucial role in the detection and exclusion of faulty GNSS measurements using the parameterized quadratic programming formulation. The two parameter tuning methods proposed are based on the fault detection property of the parameterized quadratic programming formulation. The first parameter tuning method makes use of an upper bound on the detection statistic associated with the detection property and guarantees that the false alarm probability will be at most some required value. In general, the first parameter tuning method will result in more conservative integrity risk bounds. The second parameter tuning method makes use of the detection statistic and the kernel density estimation [44] to estimate the cumulative distribution function of the detection statistic. The second parameter tuning method offers tighter integrity risk bound but the associated false alarm probability is not necessarily bounded by the required value. Both the first and the second parameter tuning methods are presented in Chapter 3.

1.4.3 Vertical Protection Level Calculation

In addition to integrity risk bound, the integrity performance of fault detection and exclusion algorithms for vertical navigation can also be evaluated through the calculation of vertical protection level. Since the vertical protection level can be interpreted as the confidence interval of the vertical position estimate, it provides a more intuitive characterization of the integrity performance as compared to the integrity risk bound. With the aim to benefit vertical navigation with the parameterized quadratic programming, the calculation of the vertical protection level for the parameterized quadratic programming is formulated. In particular, it is shown how the vertical protection level calculation for the parameterized quadratic programming

formulation can be integrated to that for the ARAIM in the case of fault detection. The formulation of the vertical protection level calculation is shown in Chapter 3, together with the vertical protection level calculation method for ARAIM in the case of detection. It is also shown in Chapter 3 how the parameterized quadratic programming formulation can be integrated to the vertical protection level calculation method for ARAIM, in the case of detection.

2. DETECTION AND EXCLUSION OF FAULTY GNSS MEASUREMENTS AND RECEIVER AUTONOMOUS INTEGRITY MONITORING

In this chapter, the problem of the detection and exclusion of faulty GNSS measurements is formulated. In particular, the RAIM and its application to detect faulty GNSS measurements are described in detail since they form a building block for the proposed PQP method. Also shown in this chapter is the calculation of both the horizontal and vertical protection levels, which can be used respectively to verify the integrity requirements for horizontal navigation and vertical navigation.

2.1 GNSS Measurement Equations

2.1.1 Pseudorange Measurements

The pseudorange measurements are the range measurements a GNSS receiver extracts from the received GNSS signals. Suppose that the received GNSS signals are indexed by i and denote the satellite transmitting the i^{th} signal by the i^{th} satellite, the pseudorange measurement of the i^{th} satellite, ρ_i, can be modeled as [45]

$$\rho_i = r(\mathbf{pos}, \mathbf{pos}_i) + b_{r,k} - b_i + d_{ion,i} + d_{tropo,i} + \mu. \tag{2.1}$$

where

$r(\mathbf{pos}_r, \mathbf{pos}_i)$ is the distance between user and the i^{th} satellite,

$\mathbf{pos}_r$ is the vector of the three space coordinates of the user,

$\mathbf{pos}_i$ is the vector of the space coordinates of the i^{th} satellite at the time the i^{th} signal is transmitted,

$b_{r,k}$ is the receiver clock bias relative to the reference time of the k^{th} satellite constellation, to which the i^{th} satellite belongs,

b_i is the satellite clock offset of the i^{th} satellite relative to the reference time of the k^{th} satellite constellation,

$d_{ion,i}$ is the ionospheric delay,

$d_{tropo,i}$ is the tropospheric delay, and

μ is the receiver thermal noise.

In (2.1), $\mathbf{pos}_i$ is considered known since it can be determined from the orbit parameters obtained from the i^{th} signal. b_i can also be obtained from the received signal, while $d_{ion,i}$ and $d_{tropo,i}$ can be estimated from the information contained in the received signal and ionosphere delay model [46] and troposphere delay models [47, 48]. Because ρ_i is provided by the receiver, what are left unknown in (2.1) are $\mathbf{pos}_r$ and b_k. Under the context of single constellation GNSS, a set of nonlinear equations can be formed with a minimum of four pseudorange measurements. Numerical methods including the nonlinear weighted least-squares estimation [49] can be applied to solve for the three components of $\mathbf{pos}_r$ and b_k.

2.1.2 Linearized Observation Equations

The strategy that is employed to solve for $\mathbf{pos}_r$ and the receiver is clock biases from the pseudorange measurements involves expanding the set of nonlinear equations using Taylor series with respective to the three components of $\mathbf{pos}_r$ and the receiver clock biases [50]. Corrections to the three components of $\mathbf{pos}_r$ and receiver clock biases are then calculated using the least squares method. The process is repeated until the estimated $\mathbf{pos}_r$ and the receiver clock biases converge. The equations resulting from the Taylor series expansion are called the linearized observation equations can be written as

$$\mathbf{y} = \mathbf{G}\mathbf{x} + \boldsymbol{\epsilon}_n. \tag{2.2}$$

In (2.2), $\mathbf{y}$ is the the vector composed of the linearized pseudorange measurements and can be obtained following the procedure reported in [51], $\mathbf{G}$ is the geometry matrix, $\mathbf{x}$ is the column vector of corrections, and $\boldsymbol{\epsilon}_n$ is the nominal error vector. For single constellation and multi-constellation GNSS, $\mathbf{G}$ and $\mathbf{x}$ take slightly different forms.

Single Constellation GNSS

For single constellation GNSS, all the received GNSS measurements come from the satellites that belong to the same constellation. Since the clocks on the satellites are synchronized to the same time frame of reference, the pseudorange measurements share an identical receiver clock bias and thus there is only one receiver clock bias to be determined. Denoting the vector of corrections to the position by $\delta\mathbf{pos}_r$ and the correction to the receiver clock bias by δb, the vector of corrections can be written as

$$\mathbf{x} = \begin{bmatrix} \delta\mathbf{pos}_r^T & \delta b \end{bmatrix}^T. \tag{2.3}$$

For the purpose of illustration, suppose that there are n_1 pseudorange measurements, all of which are indexed by the index i and all come from the satellites belonging to satellite constellation 1, the geometry matrix is of dimension $n_1 \times 4$, taking the form of

$$\mathbf{G} = \begin{bmatrix} \vdots & \vdots \\ \mathbf{los}_i^T & 1 \\ \vdots & \vdots \end{bmatrix}. \tag{2.4}$$

The $\mathbf{los}_i$ in (2.4) is the line-of-sight unit direction vector from the i^{th} satellite to the estimated user position.

Multi-Constellation GNSS

For multi-constellation, more than one receiver clock bias should be estimated. Specifically, there is an unknown receiver clock bias for each satellite constellation. Suppose that there are n_1 and n_2 pseudorange measurements from satellite constellation 1 and satellite constellation 2 respectively. Assume further that $\mathbf{G}_1$ and $\mathbf{G}_2$ are the geometry matrices associated with the linearized pseudorange measurements from only constellation 1 and those from only constellation 2. The geometry matrix associated with all the linearized pseudorange measurements is a $(n_1 + n_2) \times 5$ block matrix, constructed from the submatrices of $\mathbf{G}_1$ and $\mathbf{G}_2$

$$\mathbf{G} = \begin{bmatrix} \mathbf{G}_{n_1 \times 3} & \mathbf{1}_{n_1} & \mathbf{0}_{n_1} \\ \mathbf{G}_{n_2 \times 3} & \mathbf{0}_{n_2} & \mathbf{1}_{n_2} \end{bmatrix}. \tag{2.5}$$

where,

$$\mathbf{G}_1 = \begin{bmatrix} \mathbf{G}_{n_1 \times 3} & \mathbf{1}_{n_1} \end{bmatrix}, \tag{2.6}$$

and

$$\mathbf{G}_2 = \begin{bmatrix} \mathbf{G}_{n_2 \times 3} & \mathbf{1}_{n_2} \end{bmatrix}. \tag{2.7}$$

In (2.5), $\mathbf{0}_{n_1}$ and $\mathbf{0}_{n_2}$ are the zero vectors of the appropriate dimensions, respectively. The $\mathbf{1}_{n_1}$ and $\mathbf{1}_{n_2}$ are the column vectors of the appropriate dimensions, whose components are all equal to one. If there is a third constellation with geometry matrix

$$\mathbf{G}_3 = \begin{bmatrix} \mathbf{G}_{n_3 \times 3} & \mathbf{1}_{n_3} \end{bmatrix}, \tag{2.8}$$

then the geometry matrix can be constructed in a similar fashion

$$\mathbf{G} = \begin{bmatrix} \mathbf{G}_{n_1 \times 3} & \mathbf{1}_{n_1} & \mathbf{0}_{n_1} & \mathbf{0}_{n_1} \\ \mathbf{G}_{n_2 \times 3} & \mathbf{0}_{n_2} & \mathbf{1}_{n_2} & \mathbf{0}_{n_2} \\ \mathbf{G}_{n_3 \times 3} & \mathbf{0}_{n_3} & \mathbf{0}_{n_3} & \mathbf{1}_{n_3} \end{bmatrix}. \tag{2.9}$$

2.1.3 Detection and Exclusion of Faulty GNSS Measurements

Assume now that there a total of n_{sv} pseudorange measurements, which come from n_c satellite constellations. Assume further that the associated system of linearized observation equations is described by (2.2). Under the assumptions, the dimensions of the geometry matrix $\mathbf{G}$ are $n_{sv} \times (3 + n_c)$. In addition, the convention that is adopted is to model the nominal error vector ϵ_n as a vector whose components are independent normal random variables with zero mean. Denoting the covariance matrix of the independent normal random variables by $\mathbf{W}^{-1}$, the error vector associated with the estimated position and receiver clock biases, $\mathbf{e}$, can be expressed as [14]

$$\mathbf{e} = \mathbf{P}_0 \mathbf{G}_0^T \mathbf{W}_{\frac{1}{2}} \boldsymbol{\epsilon}_n. \tag{2.10}$$

The $\mathbf{G}_0$ in (2.10) is defined by [52]

$$\mathbf{G}_0 = \mathbf{W}_{\frac{1}{2}} \mathbf{G}, \tag{2.11}$$

where

$$\mathbf{W}_{\frac{1}{2}} \mathbf{W}_{\frac{1}{2}} = \left(\mathbf{W}^{-1}\right)^{-1}. \tag{2.12}$$

In (2.12), $\left(\mathbf{W}^{-1}\right)^{-1}$ denotes the inverse of $\mathbf{W}^{-1}$. $\mathbf{P}_0$ is defined by $\mathbf{G}_0$ through

$$\mathbf{P}_0 = \left(\mathbf{G}_0^T \mathbf{G}_0\right)^{-1}. \tag{2.13}$$

Note that such $\mathbf{P}_0$ exists when the number of measurements is large enough to estimate $\mathbf{x}$ from (2.2), using weighted least squares estimation [53]. In other words, when the number of is large enough to allow for the weighted least squares estimation of $\mathbf{x}$.

Vertical Position Error Under Nominal Conditions

If it is further assumed that the line-of-sight unit direction vectors contained in $\mathbf{G}$ are expressed in the local East-North-Up (ENU) reference frame, the third component of $\mathbf{e}$ represents the vertical position error. The vertical position error under nominal conditions can thus be written as

$$e_{v,n} = \boldsymbol{\alpha}_v^T \mathbf{P}_0 \mathbf{G}_0^T \mathbf{W}_{\frac{1}{2}} \boldsymbol{\epsilon}_n, \tag{2.14}$$

where $\boldsymbol{\alpha}_v$ is a $(3 + n_c) \times 1$ column vector, whose components vanish except for the third component being one. Note that $e_{v,n}$ is also a normal random variable such that

$$\mathrm{E}[e_{v,n}] = 0, \tag{2.15}$$

and

$$\mathrm{Var}[e_{v,n}] = \boldsymbol{\alpha}_v^T \mathbf{P}_0 \boldsymbol{\alpha}_v. \tag{2.16}$$

In (2.15) and (2.16), $\mathrm{E}[e_{v,n}]$ denotes the mean of $e_{v,n}$ and $\mathrm{Var}[e_{v,n}]$ denotes the variance of $e_{v,n}$.

Vertical Position Error with Faulty Measurements

With the existence of faulty measurements, (2.2) no longer provides an accurate model for the linearized pseudorange measurements. In cases of faulty measurements, an unknown fault vector $\mathbf{f}$ can be added and (2.2) becomes

$$\mathbf{y} = \mathbf{G}\mathbf{x} + \mathbf{f} + \boldsymbol{\epsilon}_n. \tag{2.17}$$

With the addition of the unknown fault vector $\mathbf{f}$, the vertical position error becomes

$$e_{v,f} = \boldsymbol{\alpha}_v^T \mathbf{P}_0 \mathbf{G}_0^T \mathbf{W}_{\frac{1}{2}} \Big(\mathbf{f} + \boldsymbol{\epsilon}_n \Big). \tag{2.18}$$

Similar to $e_{v,n}$, $e_{v,f}$ is also a normal random variable such that

$$\mathrm{E}[e_{v,f}] = \boldsymbol{\alpha}_v^T \mathbf{P}_0 \mathbf{G}_0^T \mathbf{W}_{\frac{1}{2}} \mathbf{f}, \tag{2.19}$$

and

$$\mathrm{Var}[e_{v,f}] = \boldsymbol{\alpha}_v^T \mathbf{P}_0 \boldsymbol{\alpha}_v. \tag{2.20}$$

Despite that $e_{v,n}$ and $e_{v,f}$ have the same variance, the mean of $e_{v,n}$ vanishes while the mean of $e_{v,f}$ is non-vanishing in general. The existence of faulty measurements degrades the distribution of vertical position error, and it motivates the detection and exclusion of faulty GNSS measurements.

Problem Statement

The detection of faulty GNSS measurements amounts to determining if the fault vector $\mathbf{f}$ in (2.17) is the zero vector or not, while the exclusion of faulty GNSS measurement amounts to determining which of the components of $\mathbf{f}$ are nonzero.

2.2 Receiver Autonomous Integrity Monitoring (RAIM)

GNSS receivers with built in RAIM capability are able to detect the existence of faulty measurements when redundant measurements are received. By redundant measurements it means that there are more measurements than that are necessary to estimate the position and receiver clock biases. The basic idea of fault detection using

the RAIM is simple. For the purpose of vertical navigation, the RAIM computes a test statistic using the vector $\mathbf{y}$ and the associated geometry matrix. Under nominal conditions, the components of $\boldsymbol{\epsilon}_n$ are independently and normally distributed with zero means and has known covariance. It is thus possible to determine the distribution functions of the RAIM test statistic. As a result, it is possible to decide upon the acceptance or rejection of the hypothesis that the fault vector $\mathbf{f}$ is the zero vector based on the likelihood of obtaining the test statistic with the calculated value [54]. Besides the simplicity in calculation, what makes the RAIM popular for the navigation of aircraft is the characterization of the RAIM integrity by the calculation horizontal and vertical protection levels

2.2.1 RAIM Test Statistic

There are three different but equivalent ways to calculate the RAIM test statistic [55], namely, the range comparison method [56], the least-squares-residual method [23], and the parity method [57]. Since the proposed PQP method is based on the parity vector $\mathbf{p}$ that is used in the parity method, the parity vector and its role in the RAIM is described in this subsection.

Parity Vector Formulation

The calculation of the parity vector $\mathbf{p}$ for a set of n_{sv} GNSS measurements involves the calculation of the parity matrix Q, which is derived from the geometry matrix. For the weighted $n_{sv} \times (3+n_c)$ geometry matrix $\mathbf{G}_0$, the parity matrix $\mathbf{Q}$ is the $(n_{sv} - 3 - n_c) \times n_{sv}$ matrix such that

$$\mathbf{Q}\mathbf{G}_0 = \mathbf{0}, \tag{2.21}$$

and

$$\mathbf{Q}\mathbf{Q}^T = \mathbf{I}. \tag{2.22}$$

In (2.21) and (2.22), $\mathbf{0}$ and $\mathbf{I}$ are the zero and the identity matrices, both of the appropriate dimensions. From the singular value decomposition [58], such parity matrix Q exists for a given weighted geometry matrix $\mathbf{G}_0$ if it is of full column rank. The condition that $\mathbf{G}_0$ has a nonempty null space hinges upon the number of received measurements. $\mathbf{G}_0$ has a nonempty null space if and only if there are redundant measurements. Numerical methods for the calculation of $\mathbf{Q}$ includes QR iterations and Jacobi iterations [59]. Once the parity matrix is found for a given weighted geometry matrix $\mathbf{G}_0$, the parity vector can be calculated using

$$\mathbf{p} = \mathbf{Q}\mathbf{W}_{\frac{1}{2}}\mathbf{y}. \tag{2.23}$$

The RAIM test statistic is defined as

$$q_{\chi^2} = \mathbf{p}^T\mathbf{p}. \tag{2.24}$$

Under nominal conditions, the parity vector is

$$\mathbf{p} = \mathbf{Q}\mathbf{W}_{\frac{1}{2}}\boldsymbol{\epsilon}_n. \tag{2.25}$$

Therefore

$$\mathrm{E}[\mathbf{p}] = \mathbf{0}, \tag{2.26}$$

and

$$\mathrm{Var}[\mathbf{p}] = \mathbf{I}. \tag{2.27}$$

It follows from (2.24), (2.25), (2.26), and (2.27) that q_{χ^2} is also a random variable and is distributed according to the central chi-squares distribution with $(n_{sv}-3-n_c)$ degrees of freedom [60].

Least-Squares-Residual Formulation

The parity vector formulation sheds light on the distribution of the RAIM test statistic q_{χ^2} and will be used in the PQP method proposed in this dissertation. However, it is not necessary to calculate the parity matrix $\mathbf{Q}$ and the parity vector $\mathbf{p}$ to use the RAIM. As reported in [57], an equivalent formulation based on the least squares residual is

$$q_{\chi^2} = \mathbf{y}^T \mathbf{W}_{\frac{1}{2}} \mathbf{R_0} \mathbf{W}_{\frac{1}{2}} \mathbf{y}, \tag{2.28}$$

where

$$\mathbf{R}_0 = \mathbf{I} - \mathbf{G}_0 \mathbf{P}_0 \mathbf{G}_0^T. \tag{2.29}$$

Note that $\mathbf{R}_0$ is the orthogonal projection matrix that projects the linearized pseudorange measurement vector $\mathbf{y}$ to the weighted least squares residual. By substituting (2.23) into (2.24) and then comparing the result with (2.28), if follows that

$$\mathbf{R}_0 = \mathbf{Q}_0^T \mathbf{Q}_0, \tag{2.30}$$

since $\mathbf{R}_0$ and $\mathbf{Q}_0^T \mathbf{Q}_0$ are symmetric.

2.2.2 RAIM Threshold Determination

Under fault-free, or nominal, condition, q_{χ^2} is distributed according to the central chi-squares distribution with $(n_{sv} - 3 - n_c)$ degrees of freedom. In other words, it is known what the cumulative distribution function of q_{χ^2} is under the fault free

conditions. When the solution of the nonlinear weighted least squares estimation has converged, the RAIM can be applied to the resulting linearized pseudorange measurements vector $\mathbf{y}$ and test for the existence of faulty measurements. To test for the existence of faulty measurements one simply calculates the RAIM test statistic from (2.28) and then calculates the likelihood of the calculated (2.28) under the fault free hypothesis. The fault-free hypothesis is accepted if the likelihood is large enough. Otherwise the fault-free hypothesis is rejected.

Probability of False Alarms and RAIM Threshold

The statement "the fault-free hypothesis is accepted if the likelihood is large enough. Otherwise the fault-free hypothesis is rejected" is not very precise. In practice, the RAIM test statistic q_{χ^2} is directly compared to the threshold T_{χ^2}. The fault-free hypothesis is accepted if and only if

$$q_{\chi^2} \leq T_{\chi^2}. \tag{2.31}$$

The RAIM threshold can be determined by the probability of false alarms P_{FA}. The probability of false alarms is defined using the cumulative distribution function of q_{χ^2} under the fault free hypothesis. Let

$$m = n_{sv} - 3 - n_c, \tag{2.32}$$

and denoting the cumulative distribution function of q_{χ^2}, under the fault free hypothesis and evaluated by q, by $CDF_{0,m}\big(q\big)$, the probability of false alarms is defined as

$$P_{FA} = 1 - CDF_{0,m}\big(T_{\chi^2}\big). \tag{2.33}$$

If D_{RAIM} is that event that

$$q_{\chi^2} > T_{\chi^2}, \tag{2.34}$$

and H_0 is the event that the fault free hypothesis is true, then P_{FA} is the conditional probability

$$P_{FA} = P(D_{RAIM}|H_0). \tag{2.35}$$

Note that the function $CDF_{0,m}$ is the cumulative distribution function of the central chi-squares distribution with m degrees of freedom, the inverse of $CDF_{0,m}$ therefore exists. Given a required probability of false alarms $P_{FA,REQ}$ and let $CDF_{0,m}^{-1}$ be the inverse of $CDF_{0,m}$, the RAIM threshold can be determined by

$$T_{\chi^2} = CDF_{0,m}^{-1}\big(1 - P_{FA,REQ}\big). \tag{2.36}$$

2.2.3 Horizontal and Vertical Protection Levels for RAIM

If the existence of faulty measurements is detected by the RAIM, then the set of received GNSS measurements is considered problematic and the position estimated obtained using the GNSS measurements should not be used for navigation. If no faulty measurement is detected, then the GNSS position estimate can be used for navigation. However, one of the necessary conditions that the GNSS estimate can be used in PBN is that the RAIM must satisfy the integrity requirement. For the RAIM, the fulfillment of integrity requirement can be checked by the calculation of the horizontal protection level for horizontal navigation and the vertical protection level for vertical navigation. Using the vertical navigation as an example and denoting the RAIM vertical protection level by vpl_{RAIM}, then the integrity requirement for vertical navigation is fulfilled only if

$$vpl_{RAIM} \leq VAL, \tag{2.37}$$

Note the various values of vertical alarm limits for different types of instrument approaches are summarized in Table 1.1.

Vertical Protection Level Calculation for RAIM

The detailed calculation of the RAIM vertical protection level can be found in [61] and it is briefly summarized here. The vertical protection level can be calculated from

$$vpl = V_{slope,max} T_{\chi^2} + k(P_{MD}) VRMS. \tag{2.38}$$

In (2.38), T_{χ^2} is calculated using (2.36). Also, P_{MD} is the desired probability of missed detections and $k(P_{MD})$ is the number of standard deviations corresponding to the $k(P_{MD})$. In addition

$$VRMS = \sqrt{\alpha_v^T \mathbf{P}_0 \alpha_v}. \tag{2.39}$$

Finally, $V_{slope,max}$ is the maximum of

$$V_{slope,i} = \frac{|\mathbf{K}_{v,i}| \sigma_i}{\sqrt{1 - (\mathbf{I} - \mathbf{R}_0)_{i,i}}}, \tag{2.40}$$

where the index i runs through all the received measurements. In (2.39), σ_i is the i^{th} diagonal component of $\mathbf{W}_{\frac{1}{2}}$ and $(\mathbf{I} - \mathbf{R}_0)_{i,i}$ is the component of $(\mathbf{I} - \mathbf{R}_0)$ in the i^{th} row and i^{th} column.

3. DETECTION AND EXCLUSION OF FAULTY GNSS MEASUREMENTS: THE PARAMETERIZED QUADRATIC PROGRAMMING (PQP) APPROACH

Detection of faulty GNSS measurements using the RAIM can be extended to exclusion. More generally, the algorithms that detect faulty GNSS measurements can be used for exclusion. To exclude faulty GNSS measurements using a detection algorithm, one simply applies the detection algorithm repeatedly and wade through all the subsets formed by the received measurements and then select the most satisfactory subset of measurements from the class of fault-free subsets. Such exhaustive search strategy has been employed and the detection and exclusion of faulty GNSS are formulated using the RAIM and ARAIM in [62]. The detection and exclusion algorithms employing exhaustive search strategy work well when the maximum number of faulty measurements to be excluded is small, but they are less ideal when the maximum number of faulty measurements to be excluded becomes moderate or large. Suppose for this moment that the goal is to exclude $n_{f,max}$ measurements for n_{sv} measurements. The number of all possible subsets, including the subset of all measurements, is

$$n_{subsets} \sum_{k=0}^{n_{f,max}} \frac{n_{sv}!}{k!(n_{sv}-k)!}. \tag{3.1}$$

Thus number of subsets is 1376 if at most 2 faulty measurements are to be excluded from 31 measurements, but it grows to become 5871 if at most 3 faulty measurements are to be excluded. In general, $n_{subsets}$ and the time cost required by the FDE algorithms which employ the exhaustive search strategy grow exponentially with increases in $n_{f,max}$.

3.1 The PQP Approach

3.1.1 An Underdetermined Linear Systems of Equations

Both determining if the fault vector $\mathbf{f}$ is the zero vector and which of the components of $\mathbf{f}$ are nonzero directly using (2.17) depend on $\mathbf{x}$. As what has been done in the RAIM, transforming from $\mathbf{y}$ to the parity vector $\mathbf{p}$ eliminates the dependence

$$\mathbf{p} = \mathbf{Q}\mathbf{W}_{\frac{1}{2}}(\mathbf{f} + \boldsymbol{\epsilon}_n). \tag{3.2}$$

Notice that (3.2) can be derived from (2.17), (2.21), and (2.23). In addition, $\mathbf{p}$ is a $(n_{sv} - m) \times 1$ column vector and $\mathbf{f}$ is a $n_{sv} \times 1$ column vector. In other words, (3.2) defines a system of underdetermined linear equations that depends only on $\mathbf{f}$, despite that the system is corrupted by noise.

l_0 and l_1 Regularizations

The problem, which is defined in (3.2), is an ill-conditioned problem since the number of the unknown variables is more than the number of the equations. If solutions exist then they may not be unique. A commonly adopted strategy is to use l_0 regularization. With an abuse of notation, denote the number of nonzero components of $\mathbf{f}$ by $\|\mathbf{f}\|_0$. After l_0 regularization, (3.2) becomes

$$\min_{\mathbf{f}} \quad \|\mathbf{f}\|_0, \tag{3.3}$$

subject to

$$\mathbf{p} = \mathbf{Q}\mathbf{W}_{\frac{1}{2}}\mathbf{f}. \tag{3.4}$$

Unfortunately, solving for the solution to (3.3) requires exhaustive search and is of non-deterministic polynomial-time (NP) hardness [38]. This nature of NP hardness makes l_0 regularization computationally intractable and leads to intensive efforts to

find good alternatives to (3.3). A direction of the efforts is the convex relaxation, which considers convex objective functions instead of the objective function in (3.2). Among the convex relaxation algorithms, the l_1 regularization is of interest

$$\min_{\mathbf{f}} \quad \|\mathbf{f}\|_1, \tag{3.5}$$

subject to

$$\mathbf{p} = \mathbf{Q}\mathbf{W}_{\frac{1}{2}}\mathbf{f}. \tag{3.6}$$

In (3.5), $\|\mathbf{f}\|_1$ denotes the l_1-norm of $\mathbf{f}$. Since $\mathbf{f}$ belongs to $\mathbb{R}^{n_{sv}-m}$,

$$\|\mathbf{f}\|_1 = \sum_{i=1}^{n_{sv}-m} |f_i|, \tag{3.7}$$

where f_i is the i^{th} component of $\mathbf{f}$. Note that the $\|\mathbf{f}\|_1$ is continuous and convex despite it is not smooth. Note also that the constraints in (3.5) define the intersection of the hyperplanes, which is also convex. As a result, (3.5) describes a convex optimization problem.

Basis Pursuit Denoising (BPDN) Formulation

An equivalent formulation of (3.5) is the basis pursuit denosing formulation [36]

$$\min_{\mathbf{f}\in\mathbb{R}^{n_{sv}}} \frac{1}{2}\|\mathbf{Q}\mathbf{W}_{\frac{1}{2}}\mathbf{f} - \mathbf{p}\|_2^2 + h\|\mathbf{W}_{\frac{1}{2}}\mathbf{f}\|_1. \tag{3.8}$$

In (3.8), h is a positive parameter to be determined. The equivalence of (3.5) and (3.8) can be seen by considering $\frac{1}{2h}$ as the Lagrange multiplier of (3.5) and (3.6).

The Parameterized Quadratic Programming (PQP) Formulation

The BPDN formulation be reformulated into the standard form of quadratic programming

$$\min_{\boldsymbol{\psi}\in\mathbb{R}^{2n_{sv}}} \quad \boldsymbol{\psi}^T\mathbf{M}\boldsymbol{\psi} + \boldsymbol{\psi}^{\mathbf{T}}\mathbf{c}, \tag{3.9}$$

subject to

$$-\boldsymbol{\psi} \leq \mathbf{0}, \tag{3.10}$$

by the change of variables (3.11), (3.12), and (3.13) [63,64]. In (3.9), $\boldsymbol{\psi}$ is the $2n_{sv}\times 1$ column vector, which is the concatenating of the two $n_{sv}\times 1$ column vectors $\mathbf{f}^+$ and $\mathbf{f}^-$

$$\boldsymbol{\psi} = \begin{bmatrix} \mathbf{f}^+ \\ \mathbf{f}^- \end{bmatrix}. \tag{3.11}$$

Each component of $\mathbf{f}^+$ is obtained by comparing the corresponding component of $\mathbf{f}$ and zero. Denoting f_i^+ and f_i the i^{th} components of $\mathbf{f}^+$ and $\mathbf{f}$ respectively, then

$$f_i^+ = \max(f_i, 0), \tag{3.12}$$

where $\max(f_i, 0)$ equals the larger of f_i and zero. f_i^- is similarly defined by

$$f_i^- = \max(-f_i, 0). \tag{3.13}$$

With the change of variables (3.11), (3.12), and (3.13), the $\mathbf{M}$ and $\mathbf{c}$ in (3.9) are

$$\mathbf{M} = \frac{1}{2}\begin{bmatrix} \mathbf{I} \\ -\mathbf{I} \end{bmatrix} \mathbf{W}_{\frac{1}{2}}\mathbf{Q}^T\mathbf{Q}\mathbf{W}_{\frac{1}{2}} \begin{bmatrix} \mathbf{I} & -\mathbf{I} \end{bmatrix}, \tag{3.14}$$

and

$$\mathbf{c} = -\begin{bmatrix} \mathbf{I} \\ -\mathbf{I} \end{bmatrix} \mathbf{W}_{\frac{1}{2}}\mathbf{Q}^T\mathbf{p} + h\begin{bmatrix} \mathbf{I} \\ \mathbf{I} \end{bmatrix} \mathbf{W}_{\frac{1}{2}}\mathbf{d}. \tag{3.15}$$

In (3.15), $\mathbf{d}$ is the $n_{sv}\times 1$ column vector whose components are all equal to one. Given a parameter h, the parameterized quadratic programming problem (3.9) can

be formed and then solved by numerical methods, for example, the interior-point methods [65, 66]. Suppose that $\hat{\boldsymbol{\psi}}$ is the solution to (3.9). Assume also that

$$\hat{\mathbf{f}}^{+} = \begin{bmatrix} \mathbf{I} & \mathbf{0} \end{bmatrix} \hat{\boldsymbol{\psi}}, \tag{3.16}$$

and

$$\hat{\mathbf{f}}^{-} = \begin{bmatrix} \mathbf{0} & \mathbf{I} \end{bmatrix} \hat{\boldsymbol{\psi}}, \tag{3.17}$$

then the solution to (3.8) is

$$\hat{\mathbf{f}} = \hat{\mathbf{f}}^{+} - \hat{\mathbf{f}}^{-}. \tag{3.18}$$

3.1.2 The PQP Algorithm

The proposed PQP approach for detection and exclusion of faulty GNSS measurements can be formulated using the algorithm below.

Algorithm 1 The PQP Algorithm

Calculate $\mathbf{W}_{\frac{1}{2}}$ such that (2.12) holds.
Calculate $\mathbf{G}_0$ according to (2.11).
Calculate $\mathbf{Q}$ such that (2.21) and (2.22) hold.
Calculate $\mathbf{p}$ according to (2.23).
Determine the PQP parameter h.
Calculate $\mathbf{M}$ and $\mathbf{c}$ according to (3.14) and (3.15).
Solve for $\hat{\boldsymbol{\psi}}$, the solution to (3.9).
Calculate $\hat{\mathbf{f}}$ according to (3.16), (3.17), and (3.18).
if $\hat{\mathbf{f}} = \mathbf{0}$ **then**
  Claim no detection.
  (Optional) calculate integrity risk bound or protection level.
else
  Calculate $\mathbf{A}_{ex}$ and $\mathbf{B}_{ex}$
  Calculate $q_{\chi^2,ex}$ accordint to (3.63), with index j replaced by the value of the index ex.
  Calculate T_{ex} accordint to (3.94), with index j replaced by the value of the index ex.
  if $q_{\chi^2,ex} \leq T_{ex}^2$ **then**
    Claim exclusion.
    (Optional) calculate integrity risk bound or protection level.
  else
    Claim detection.
  end if
end if

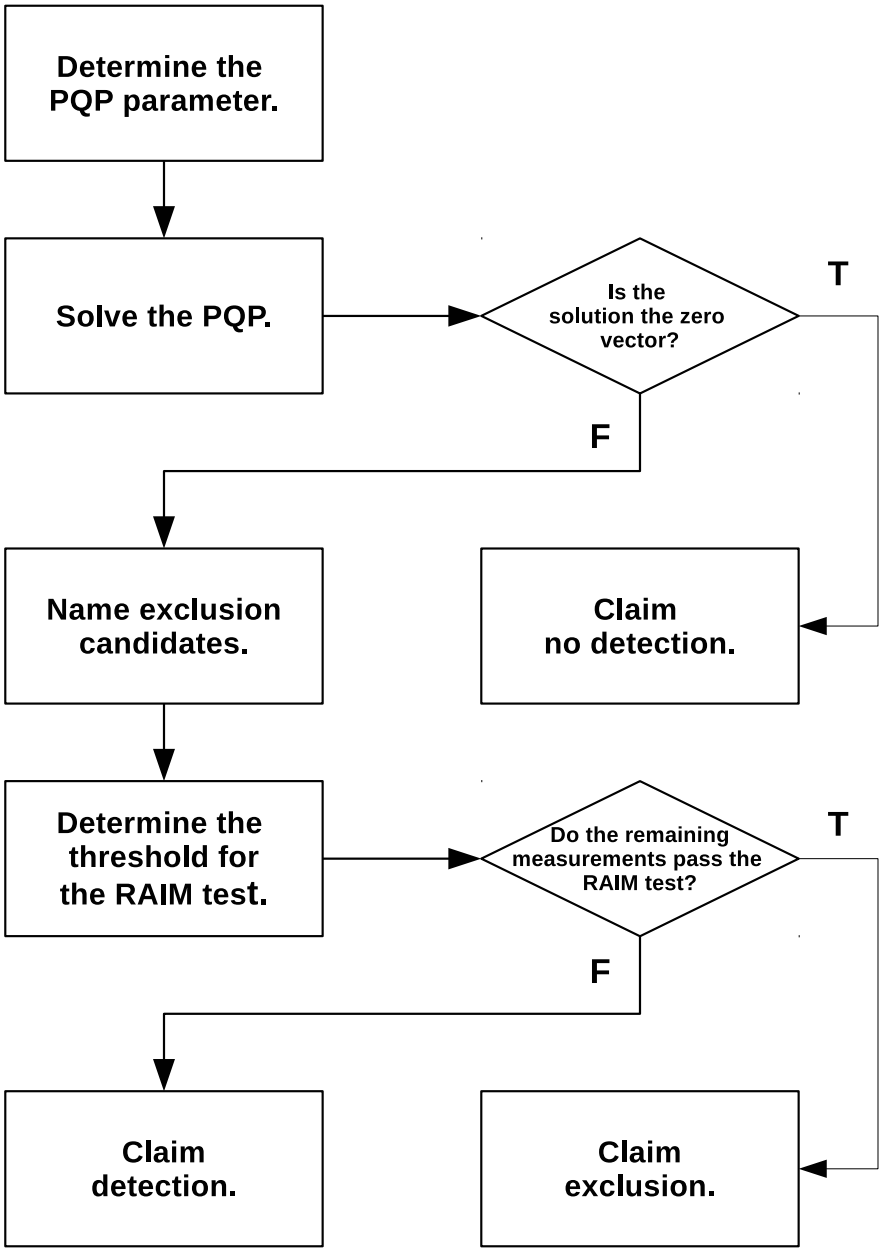

Figure 3.1. The parameterized quadratic programming (PQP) method summarized in a flowchart.

In a nutshell, an instance of problem (3.8) can be constructed with a set of received GNSS measurements and then it can be solved. If the solution $\hat{\mathbf{f}}$ is the zero vector then the PQP approach claims that the set of measurements is fault-free. Otherwise, a new linear system of equations is formed by excluding the GNSS measurements that are associated with the nonzero components of $\hat{\mathbf{f}}$. The RAIM test statistic $q_{\chi^2,ex}$ and the RAIM threshold $T_{\chi^2,ex}$ are calculated for the RAIM detection test. If the new system passes the RAIM detection test, the new measurements that are associated with the new system are claimed to be fault-free by the PQP approach. If the new system fails to pass the test then the PQP approach claims the existence of faulty measurements but is not able to exclude the faulty measurements. Figure 3.1 summarizes the PQP approach in the flowchart. Up to this point, some topics related to the PQP approach remain not clarified. More precisely, the impact exclusion has on position estimate, the tuning of the parameter h, the definition of integrity risk for the PQP approach, and the calculation of integrity risk bounds or protection levels for the PQP approach. Therefore, the rest of this chapter is devoted to the aforementioned topics.

3.2 Two Parameter Tuning Methods

The first topic that is dealt with is the tuning of the parameter h. Two parameter tuning methods are proposed in this dissertation, both of which are based on the detection property of the PQP approach. In particular, associated with the PQP approach there exist a test statistic and detection threshold for fault detection. The PQP parameter is closely related with the detection threshold associated with the PQP approach, which in turn depends upon the necessary and sufficient conditions for $\hat{\mathbf{f}}$ to be equal to the zero vector.

3.2.1 The Detection Property of the PQP Approach

The Existence of the Solutions to (3.8)

A sufficient condition to establish the existence of the solution to (3.9) and (3.10), and thus (3.8), is what follows [67, 68]. If the feasible set of (3.9) is nonempty and the optimal value is bounded below, then the minimum is attained in the feasible set. The proof of the existence of solution can be found in [67,69]. Notice that the feasible set of the problem in (3.9) and (3.10) is nonempty and that (3.8) and the problem in (3.9) and (3.10) have identical optimal values. Notice that they are bounded below. The existence of the solutions to (3.8) and the problem in (3.9) and (3.10) can be estabilished.

Characterization of $\hat{\mathbf{f}}$

While (3.9) is constrained by (3.10), (3.8) is unconstrained and it could be solved by directly differentiating the objective function and then checking the objection function values at the point where the derivatives vanish, if the objective function was differentiable. However, the l_1-norm is not smooth because its first derivative does not exist at the origin. Fortunately, the objective function is convex and (3.8) can be approached by the subgradient method [70, 71]. If the objective function of (3.8) is denoted by $F_{obj} : \mathbb{R}^{n_{sv}} \to \mathbb{R}$, then the epigraph of F_{obj} is the set

$$\text{epi } F_{obj} = \left\{ (\mathbf{f}^T, t)^T | \mathbf{f} \in \text{dom } F_{obj}, F_{obj}(\mathbf{f}) \leq t \right\}, \tag{3.19}$$

where dom F_{obj} is the domain of F_{obj}. A vector $\mathbf{g}$ is a subgradient at some point $\mathbf{f}$ in dom F_{obj} if and only if the augmented vector $\left(\mathbf{g}^T, -1\right)^T$ is the normal vector of a supporting hyperplane of epi F_{obj} at $\left(\mathbf{f}^T, F_{obj}(\mathbf{f})\right)^T$ [66]. For (3.8)

$$F_{obj}(\mathbf{f}) = \frac{1}{2}\|\mathbf{Q}\mathbf{W}_{\frac{1}{2}}\mathbf{f} - \mathbf{p}\|_2^2 + h\|\mathbf{W}_{\frac{1}{2}}\mathbf{f}\|_1. \tag{3.20}$$

A vector $\mathbf{f}$ is the solution to (3.8) if and only if the zero vector is a subgradient of F_{obj} at $\mathbf{f}$. Therefore

$$\mathbf{W}_{\frac{1}{2}}\mathbf{Q}^T(\mathbf{Q}\mathbf{W}_{\frac{1}{2}}\hat{\mathbf{f}} - \mathbf{p}) + h\mathbf{W}_{\frac{1}{2}}\mathbf{u} = \mathbf{0}. \tag{3.21}$$

In (3.21), $\mathbf{u}$ is the subgradient of $\|\mathbf{W}_{\frac{1}{2}}\mathbf{f}\|_1$. To be more specific,

$$\mathbf{u}^T\mathbf{W}_{\frac{1}{2}}\hat{\mathbf{f}} = \|\mathbf{W}_{\frac{1}{2}}\hat{\mathbf{f}}\|_1, \tag{3.22}$$

and

$$\|\mathbf{u}\|_\infty \leq 1. \tag{3.23}$$

Necessary and Sufficient Conditions on h

To determine the necessary and sufficient conditions on h such that $\hat{\mathbf{f}}$ vanishes, let

$$\hat{\mathbf{f}} = \mathbf{0}, \tag{3.24}$$

and search for h and $\mathbf{u}$ that satisfy (3.22) and (3.23). Now, if

$$h \geq \|\mathbf{Q}^T\mathbf{p}\|_\infty, \tag{3.25}$$

and

$$\mathbf{u} = \frac{1}{h}\mathbf{Q}^T\mathbf{p}, \tag{3.26}$$

then (3.21), (3.22), and (3.23) are satisfied. As a result, (3.25) is the necessary and sufficient conditions on h such that $\hat{\mathbf{f}}$ vanishes. This connection between the detection and the estimation of the l_2-l_1 regularized criterion used in BPDN is pointed out in [72]. The detection property of the PQP method is a manifestation of such

connection. In particular, note that the PQP method claims that the set of all received measurements is fault-free, or equivalently it claims no detection, only when $\hat{\mathbf{f}}$ equals $\mathbf{0}$. At the same time, $\hat{\mathbf{f}}$ equals $\mathbf{0}$ if and only if (3.25) is satisfied. The PQP parameter h and $\|\mathbf{Q}^T\mathbf{p}\|_\infty$ can therefore be considered as the detection threshold and the test statistic respectively. The detection property provides a perspective for parameter tuning. That is, if the probability distribution function of $\|\mathbf{Q}^T\mathbf{p}\|_\infty$ is known, under the assumption that the measurements are fault-free, then it is possible to tune the threshold, or equivalently the PQP parameter h, such that the probability of false alarms stays below some required value.

3.2.2 Parameter Tuning: Bounding the Probability of False Alarms

Tuning the PQP parameter h by bounding the probability of false alarms is encapsulated by

$$h^2 = \chi^{-2}\big(1 - P_{FA,REQ}, n_{sv} - m\big), \tag{3.27}$$

where $\chi^{-2}\big(1-P_{FA,REQ}, n_{sv}-m\big)$ is the inverse of the cumulative distribution function of the central Chi-squared distribution with $n_{sv} - m$ degrees of freedom and $P_{FA,REQ}$ is the required upper bound on the probability of false alarms. The rest of this subsection is devoted to explain the parameter tuning method shown in (3.27).

From Figure 3.1, the PQP method claims no fault is detected is the set of all measurements (no detection) if and only if $\hat{\mathbf{f}}$ is the zero vector. The PQP method alarms the users, either of detection or exclusion, if $\hat{\mathbf{f}}$ is not the zero vector. In this sense, the probability of false alarms is defined as the conditional probability that $\hat{\mathbf{f}}$ is not the zero vector, under the condition that $\mathbf{f}$ is actually the zero vector. Suppose for now that a value of the parameter h is given, it will be shown what the probability of false alarms associated with the given h is and how an upper bound can be determined. The upper bound on the probability of false alarms in turn bridges the parameter tuning method that is presented in this subsection. From (3.25), it

is suggested that h and $\|\mathbf{Q}^T\mathbf{p}\|_\infty$ should be considered as the test threshold and the test statistic, respectively. The PQP method claims no detection if and only if the threshold bounds the test statistic from the above. The conditional probability that $\hat{\mathbf{f}}$ is not the zero vector, under the condition that $\mathbf{f}$ is actually the zero vector

$$P_{FA}(h) = P\big(h \leq \|\mathbf{Q}^T\mathbf{p}\|_\infty | \mathbf{f} = \mathbf{0}\big). \tag{3.28}$$

(3.28) says that the probability of false alarms is a function of h and can be constructed if the distribution of the random variable $\|\mathbf{Q}^T\mathbf{p}\|_\infty$, under the condition that $\mathbf{f}$ vanishes, is known. Unfortunately, $\mathbf{Q}^T\mathbf{p}$ is a normal random vector with correlated components and it is generally difficult to determine the distribution of $\|\mathbf{Q}^T\mathbf{p}\|_\infty$. The proposed parameter tuning method in this and the upcoming subsections consequently revolve around this issue. Consider the relation

$$\|\mathbf{Q}^T\mathbf{p}\|_\infty \leq \|\mathbf{Q}^T\mathbf{p}\|_2. \tag{3.29}$$

It follows that the event

$$h \leq \|\mathbf{Q}^T\mathbf{p}\|_\infty \tag{3.30}$$

implies the event

$$h \leq \|\mathbf{Q}^T\mathbf{p}\|_2. \tag{3.31}$$

Thus,

$$P\big(h \leq \|\mathbf{Q}^T\mathbf{p}\|_\infty\big) \leq P\big(h \leq \|\mathbf{Q}^T\mathbf{p}\|_2\big), \tag{3.32}$$

and

$$P_{FA}(h) \leq P\big(h \leq \|\mathbf{Q}^T\mathbf{p}\|_2 | \mathbf{f} = \mathbf{0}\big). \tag{3.33}$$

Because $\mathbf{Q}$ is selected so that $\mathbf{Q}\mathbf{Q}^T$ is the identity matrix, (3.31) is equivalent to

$$h^2 \leq \mathbf{p}^T\mathbf{p}. \tag{3.34}$$

Under the assumption that $\mathbf{f}$ vanishes, $\mathbf{p}^T\mathbf{p}$ distributes according to the central Chi-squared distribution with $n_{sv} - m$ degrees of freedom [60]. Note that it is possible to tune h so that

$$P\big(h^2 \leq \mathbf{p}^T\mathbf{p}|\mathbf{f} = \mathbf{0}\big) \leq P_{FA,REQ} \tag{3.35}$$

holds. If h is tuned such that (3.35) holds, then it follows from (3.33) that

$$P_{FA}(h) \leq P_{FA,REQ}. \tag{3.36}$$

3.2.3 Parameter Tuning: Using Kernel Density Estimation

Despite that it is difficult to determine analytically how $\|\mathbf{Q}^T\mathbf{p}\|_\infty$ distribute, it is possible to numerically construct the cumulative distribution of $\|\mathbf{Q}^T\mathbf{p}\|_\infty$, under the assumption that $\mathbf{f}$ vanishes. Under such assumption,

$$\mathbf{Q}^T\mathbf{p} = \mathbf{Q}^T\mathbf{Q}\mathbf{W}_{\frac{1}{2}}\boldsymbol{\epsilon}_n. \tag{3.37}$$

For a given satellite geometry and nominal measurement model, samples of $\mathbf{Q}^T\mathbf{p}$ can be simulated, which in turn can be used to obtain samples of $\|\mathbf{Q}^T\mathbf{p}\|_\infty$. Using the samples of $\|\mathbf{Q}^T\mathbf{p}\|_\infty$, a numerical approximation of the cumulative distribution function of $\|\mathbf{Q}^T\mathbf{p}\|_\infty$ can be constructed by kernel density estimation (KDE) [44], together with a selected kernel function.

3.2.4 Remarks on the Parameter Tuning Methods

While tuning the PQP parameter by bounding the probability of false alarms can be efficiently done and is suitable for real-time applications, it will been seen from the simulation results in the next chapter that tuning the PQP parameter by bounding the probability of false alarms generally leads to more conservative integrity performance. On the contrary, tuning the PQP parameter using KDE results in better integrity performance but it requires the a certain amount of simulated samples or GNSS measurements that are known to be fault-free. In addition, there's no guarantee that the resulting probability of false alarm will be bounded by the required probability of false alarms. Tuning the parameter using KDE is therefore not suitable for real-time applications in this sense. Instead, tuning the parameter using KDE provides a means of assessing the expected integrity performance of the PQP method. If the expected integrity performance is similar to the more conservative one resulted from the bounding the probability of false alarms method, then there's no need to pursuit further parameter tuning method for real-time applications. Another remark is for every instance of the problem in (3.9) and (3.10), an equivalent support vector machine (SVM) [73, 74] can be constructed [75, 76]. The equivalence between the SVM and the PQP suggests that it may be possible for the PQP approach to benefit from the researches and studies conducted for the SVM.

3.2.5 An Equivalent Support Vector Machine

As reported in [75], there's an equivalence between sparse approximation and support vector machines (SVM). Since the PQP method stems from sparse approximation, the equivalence leads to an equivalent SVM for the detection and exclusion of faulty GNSS measurements. Given a set of N data points $\left\{(\boldsymbol{\omega_i}, z_i)\right\}_{i=1}^{N}$ which are sampled from a function

$$z = f\big(\boldsymbol{\omega}\big), \tag{3.38}$$

the SVM finds an approximation of the function f of the form

$$f\big(\boldsymbol{\omega}\big) = \sum_{i=1}^{\infty} c_i \phi_i(\boldsymbol{\omega}). \tag{3.39}$$

In (3.39), each ϕ_i is a known function that comes from an set of basis function of a Reproducing Kernel Hilbert Space (RKHS) [77] $\mathcal{H}$ and the corresponding c_i is what is to be sought. The strategy employed to determine the countably infinite set of coefficients, using only a finite number of data points, is to minimize the cost function

$$\min_{f \in \mathcal{H}} C \sum_{i=1}^{N} V\big(z_i - f(\boldsymbol{\omega_i})\big) + \frac{1}{2}\Psi\big(f\big). \tag{3.40}$$

In (3.40), C is a positive constant, and $V\big(z_i - f(\boldsymbol{\omega_i})\big)$ is an error function whose input argument is the difference between z_i and $f(\boldsymbol{\omega_i})$. Finally,

$$\Psi\big(f\big) = \sum_{i=1}^{\infty} \frac{c_i^2}{\lambda_i}, \tag{3.41}$$

where each λ_i belongs to a decreasing sequence of positive constants. It is shown in [75] that the solution to (3.40) is always

$$f\big(\boldsymbol{\omega}\big) = \sum_{i=1}^{N} a_i K\big(\boldsymbol{\omega}, \boldsymbol{\omega_i}\big), \tag{3.42}$$

regardless of the error function used. The $K\big(\boldsymbol{\omega}, \boldsymbol{\omega_i}\big)$ in (3.46) is the kernel function associated with the RKHS $\mathcal{H}$,

$$K\big(\boldsymbol{\omega}, \boldsymbol{\omega_i}\big) = \sum_{j=1}^{\infty} \lambda_j \psi(\boldsymbol{\omega})_j \psi(\boldsymbol{\omega}_i)_j. \tag{3.43}$$

Given $\boldsymbol{\omega}$ and $\boldsymbol{\omega}_i$, the calculation of $K\big(\boldsymbol{\omega}, \boldsymbol{\omega_i}\big)$, according to (3.43), involves summing a infinite number of terms. Fortunately, the theory of RKHS says that such calculations can be avoided if the RKHS $\mathcal{H}$ is known. For example, if $\mathcal{H}$ is the RKHS of Gaussian radial basis function, then the kernel function is of the form

$$K\big(\boldsymbol{\omega}, \boldsymbol{\omega_i}\big) = \exp(-\|\boldsymbol{\omega} - \boldsymbol{\omega_i}\|_2^2). \tag{3.44}$$

It is further shown if the error function is the ϵ-insensitive cost function [78] according

$$V\big(z\big) = |z|_\epsilon \begin{cases} 0 & \text{if } |z| < \epsilon \\ |z| - \epsilon & \text{otherwise} \end{cases}, \tag{3.45}$$

then the solution to (3.40) is

$$f\big(\boldsymbol{\omega}, \boldsymbol{\alpha}_+, \boldsymbol{\alpha}_-\big) = \sum_{i=1}^{N} \big(\alpha_i^+ - \alpha_i^-\big) K\big(\boldsymbol{\omega}, \boldsymbol{\omega_i}\big), \tag{3.46}$$

where α_i^+ and α_i^- are the i^{th} components of $\boldsymbol{\alpha}_+$ and $\boldsymbol{\alpha}_-$, respectively. Also, $\boldsymbol{\alpha}_+$ and $\boldsymbol{\alpha}_-$ are to solution to the QP

$$\begin{aligned} \min_{\boldsymbol{\alpha}_+, \boldsymbol{\alpha}_-} \quad & \epsilon \sum_{i=1}^{N} \big(\alpha_i^+ + \alpha_i^-\big) \\ & - \sum_{i=1}^{N} z_i \big(\alpha_i^+ - \alpha_i^-\big) \\ & + \frac{1}{2} \sum_{i,j=1}^{N} \big(\alpha_i^+ - \alpha_i^-\big)\big(\alpha_j^+ - \alpha_j^-\big) K\big(\boldsymbol{\omega}_i, \boldsymbol{\omega_j}\big) \end{aligned}, \tag{3.47}$$

subject to

$$0 \leq \alpha_i^+ \leq C, \forall i \in \{1 \ldots N\}, \tag{3.48}$$

$$0 \leq \alpha_i^- \leq C, \forall i \in \{1 \ldots N\}, \tag{3.49}$$

and

$$\alpha_i^+ \alpha_i^- = 0, \forall i \in \{1 \ldots N\}, \tag{3.50}$$

Comparing (3.47), (3.48), (3.49), and (3.50) with (3.9), (3.10), (3.14), and (3.15), it shows that

$$\alpha_i^+ = w_i f_i^+, \tag{3.51}$$

$$\alpha_-^+ = w_i f_i^-, \tag{3.52}$$

and

$$K\big(\boldsymbol{\omega}_i, \boldsymbol{\omega}_{\boldsymbol{j}}\big) = M_{i,j}, \tag{3.53}$$

where $M_{i,j}$ is the component of the in the i^{th} row and the j^{th} column of $\mathbf{Q}^T\mathbf{Q}$. In addition,

$$\mathbf{z} = \mathbf{Q}^T\mathbf{p}, \tag{3.54}$$

and

$$\epsilon = h. \tag{3.55}$$

3.3 The Integrity of the PQP Approach

The PQP approach detects and excludes faulty GNSS measurements with a goal to improve the distribution of vertical position error. With the weighted least squares estimation, the vertical position error of the system (2.17) is the random variable $e_{v,f}$ in (2.18). Suppose now that a subset of measurements of $\mathbf{y}$ are excluded and a new system is formed

$$\mathbf{y}_{ex} = \mathbf{B}_{ex}^T\mathbf{y} = \mathbf{B}_{ex}^T\big(\mathbf{G}\mathbf{x} + \mathbf{f} + \boldsymbol{\epsilon}_n\big). \tag{3.56}$$

In (3.56), $\mathbf{B}_{ex}$ is the rectangular matrix, which is composed of zeros and ones, such that $\mathbf{B}_{ex}^T\mathbf{y}$ is the vector of measurements that are to be retained after exclusion. Note that $\mathbf{B}_{ex}$ can be constructed by the inspecting the indices of the nonzero components

of $\hat{\mathbf{f}}$. The vertical position error associated with the weighted least squares estimation is

$$e_{v,f,ex} = \boldsymbol{\alpha}_v^T \mathbf{P}_{ex} \mathbf{G}_{ex}^T \mathbf{B}_{ex}^T \mathbf{W}_{\frac{1}{2}} \big(\mathbf{f} + \boldsymbol{\epsilon}_n\big). \tag{3.57}$$

In order to write down expressions of $\mathbf{G}_{ex}$ and $\mathbf{P}_{ex}$ explicitly, $\mathbf{B}_{ex,\frac{1}{2}}$ is introduced

$$\mathbf{B}_{ex,\frac{1}{2}} = \mathbf{W}_{\frac{1}{2}} \mathbf{B}_{ex}. \tag{3.58}$$

After $\mathbf{B}_{ex,\frac{1}{2}}$ is defined,

$$\mathbf{G}_{ex} = \mathbf{B}_{ex,\frac{1}{2}}^T \mathbf{G}, \tag{3.59}$$

and

$$\mathbf{P}_{ex} = \big(\mathbf{G}_{ex}^T \mathbf{G}_{ex}\big)^{-1}. \tag{3.60}$$

Now, $e_{v,f,ex}$ is a normal random variable with mean

$$\mathrm{E}[e_{v,f,ex}] = \boldsymbol{\alpha}_v^T \mathbf{P}_{ex} \mathbf{G}_{ex}^T \mathbf{B}_{ex}^T \mathbf{W}_{\frac{1}{2}} \mathbf{f}, \tag{3.61}$$

and variance

$$\mathrm{Var}[e_{v,f,ex}] = \boldsymbol{\alpha}_v^T \mathbf{P}_{ex} \boldsymbol{\alpha}_v. \tag{3.62}$$

If the all the faulty measurements are excluded by $\mathbf{B}_{ex}$ then $\mathbf{B}_{ex}^T \mathbf{f}$ vanishes and so does $\mathrm{E}[e_{v,f,ex}]$. If $\mathbf{B}_{ex}$ removes all the faulty measurements in $\mathbf{y}$, then the exclusion improves the distribution of vertical position error by reducing its mean to zero. However, two problems arise. Firstly, there's no guarantee that the variance of the vertical position error will necessarily decrease. That is, $\mathrm{Var}[e_{v,f,ex}]$ is not necessarily smaller than $\mathrm{Var}[e_{v,f}]$, even if $\mathbf{B}_{ex}^T \mathbf{f}$ is the zero vector. Secondly, $\mathbf{B}_{ex}^T \mathbf{f}$ will not

necessarily be the zero vector. These problems justify the need of the mathematical characterizations of the integrity and continuity risks of the PQP approach.

3.3.1 The Building Blocks and the Integrity and Continuity Risks of FDE

In order to introduce the general integrity and continuity risks, some events and the associated remarks, which serve as the building blocks of the integrity and continuity risks, are introduced.

The Events

H_0: the fault-free hypothesis, which is the event that f is the zero vector.

H_i: the ith of the total n_{FH} fault hypotheses. Suppose, for example, that there are totally 31 measurements and that H_{32} is the fault hypothesis such that the measurements associated with the first and second components of $\mathbf{y}$ are faulty, then H_{32} is the event that all the components of $\mathbf{f}$ equal zero, except that the first and second components of $\mathbf{f}$ are nonzero.

ND: the event that the PQP method claims no detection in Figure 3.1. Since the PQP method claims no detection if and only if $\hat{\mathbf{f}}$ is the zero vector, ND is characterized by (3.25). Note that this event depends on the PQP parameter h.

D: the complement of ND.

E_j: the event such that

$$q_{\chi^2,j} = \mathbf{y}^T \mathbf{B}_{j,\frac{1}{2}} \mathbf{R}_j \mathbf{B}_{j,\frac{1}{2}}^T \mathbf{y} \leq T_j^2. \tag{3.63}$$

In (3.63)

$$\mathbf{B}_{j,\frac{1}{2}} = \mathbf{W}_{\frac{1}{2}} \mathbf{B}_j, \tag{3.64}$$

where $\mathbf{B}_j$ is the rectangular matrix which is composed of zeros and ones. In addition, $\mathbf{B}_j^T\mathbf{y}$ is the vector of measurements that are assumed to be faulty-free by H_j. Also

$$\mathbf{G}_j = \mathbf{B}_{j,\frac{1}{2}}^T\mathbf{G}, \tag{3.65}$$

$$\mathbf{P}_j = \left(\mathbf{G}_j^T\mathbf{G}_j\right)^{-1}, \tag{3.66}$$

and

$$\mathbf{R}_j = \mathbf{I} - \mathbf{G}_j\mathbf{P}_j\mathbf{G}_j^T. \tag{3.67}$$

Note that the T_j^2 is a parameter that acts as the threshold, just like h. The determination of T_j^2 depends on the required upper limit on continuity risk and is defined in (3.94).

$\overline{ND}$: the event such that

$$h \geq \frac{1}{\sqrt{n_{sv}}}\|\mathbf{Q}^T\mathbf{p}\|_2. \tag{3.68}$$

HI_0: the event such that the magnitude the vertical position error associated with the weighted least squares estimate resulted from all the received measurements, shown in (2.18), exceeds a given alarm limit l_{al}. That is

$$|e_{v,f}| = |\boldsymbol{\alpha}_v^T\mathbf{P}_0\mathbf{G}_0^T\mathbf{W}_{\frac{1}{2}}\left(\mathbf{f} + \boldsymbol{\epsilon}_n\right)| > l_{al}. \tag{3.69}$$

HI_j: the event such that the magnitude the vertical position error, that is associated with the weighted least squares estimate resulted from the measurements that are assumed to be fault-free by H_j, exceeds l_{al}. That is,

$$|e_{v,f,j}| = |\boldsymbol{\alpha}_v^T\mathbf{P}_j\mathbf{G}_j^T\mathbf{B}_{j,\frac{1}{2}}\left(\mathbf{f} + \boldsymbol{\epsilon}_n\right)| > l_{al}. \tag{3.70}$$

Two Remarks on the Events

Firstly, ND implies $\overline{ND}$, since

$$n_{sv}\|\mathbf{Q}^T\mathbf{p}\|_\infty^2 \geq \|\mathbf{Q}^T\mathbf{p}\|_2^2. \tag{3.71}$$

Consquently,

$$P(ND) \leq P(\overline{ND}), \tag{3.72}$$

where $P(ND)$ and $P(\overline{ND})$ denote the probabilities of ND and $\overline{ND}$ respectively. Secondly, HI_0 and $\overline{ND}$ are independent. To prove the independence, the following result in used [79] Let $\mathbf{v}_1$ be a $n_1 \times 1$ normal random vector and $\mathbf{v}_2$ be a $n_2 \times 1$ normal random vector. Consider the normal random vector

$$\mathbf{v} = \begin{bmatrix} \mathbf{v}_1 \\ \mathbf{v}_2 \end{bmatrix}, \tag{3.73}$$

then $\mathbf{v}_1$ and $\mathbf{v}_2$ are independent if and only if the covariance of $\mathbf{v}_1$ and $\mathbf{v}_2$ vanishes. Now, if

$$\mathbf{v}_1 = \boldsymbol{\alpha}_v^T\mathbf{P}_0\mathbf{G}_0^T\mathbf{W}_{\frac{1}{2}}\big(\mathbf{f} + \boldsymbol{\epsilon}_n\big), \tag{3.74}$$

$$\mathbf{v}_2 = \mathbf{Q}^T\mathbf{p} = \mathbf{Q}^T\mathbf{Q}\mathbf{W}_{\frac{1}{2}}\big(\mathbf{f} + \boldsymbol{\epsilon}_n\big), \tag{3.75}$$

then

$$\mathbf{v} = \begin{bmatrix} \boldsymbol{\alpha}_v^T\mathbf{P}_0\mathbf{G}_0^T\mathbf{W}_{\frac{1}{2}} \\ \mathbf{Q}^T\mathbf{Q}\mathbf{W}_{\frac{1}{2}} \end{bmatrix} \big(\mathbf{f} + \boldsymbol{\epsilon}_n\big), \tag{3.76}$$

is a normal random vector. Denote the mean of $\mathbf{v}_1$ by

$$\mu_{\mathbf{v},\mathbf{1}} = \boldsymbol{\alpha}_v^T\mathbf{P}_0\mathbf{G}_0^T\mathbf{W}_{\frac{1}{2}}\mathbf{f}, \tag{3.77}$$

and the mean of $\mathbf{v}_2$ by

$$\mu_{v,2} = \mathbf{Q}^T\mathbf{Q}\mathbf{W}_{\frac{1}{2}}\mathbf{f}, \tag{3.78}$$

the covariance of $\mathbf{v}_1$ and $\mathbf{v}_2$

$$cov(\mathbf{v}_1, \mathbf{v}_2) = E\big(\mathbf{v}_1 - \mu_{v,1}\big)\big(\mathbf{v}_2 - \mu_{v,2}\big)^T \tag{3.79}$$

vanishes because $\mathbf{Q}$ is selected such that (2.21) holds. Therefore HI_0 and $\overline{ND}$ are independent and

$$P\big(HI_0, \overline{ND}\big) = P\big(HI_0\big)P\big(\overline{ND}\big). \tag{3.80}$$

Similarly, HI_j and E_j are independent. Let

$$\mathbf{u}_1 = \boldsymbol{\alpha}_v^T\mathbf{P}_j\mathbf{G}_j^T\mathbf{B}_{j,\frac{1}{2}}\big(\mathbf{f} + \boldsymbol{\epsilon}_n\big), \tag{3.81}$$

$$\mathbf{u}_2 = \big(\mathbf{B}_{j,\frac{1}{2}}\mathbf{R}_j\mathbf{B}_{j,\frac{1}{2}}^T\big)^{\frac{1}{2}}\big(\mathbf{f} + \boldsymbol{\epsilon}_n\big), \tag{3.82}$$

where $\big(\mathbf{B}_{j,\frac{1}{2}}\mathbf{R}_j\mathbf{B}_{j,\frac{1}{2}}^T\big)^{\frac{1}{2}}$ denotes the positive square root of the matrix $\mathbf{B}_{j,\frac{1}{2}}\mathbf{R}_j\mathbf{B}_{j,\frac{1}{2}}^T$. Also, let

$$\mathbf{u} = \begin{bmatrix} \mathbf{u}_1 \\ \mathbf{u}_2 \end{bmatrix}, \tag{3.83}$$

If follows that $\mu_{\mathbf{u},\mathbf{1}}$ and $\mu_{u,2}$ are

$$\mu_{\mathbf{u},\mathbf{1}} = \boldsymbol{\alpha}_v^T\mathbf{P}_j\mathbf{G}_j^T\mathbf{B}_{j,\frac{1}{2}}\mathbf{f}, \tag{3.84}$$

and

$$\mu_{u,2} = \big(\mathbf{B}_{j,\frac{1}{2}}\mathbf{R}_j\mathbf{B}_{j,\frac{1}{2}}^T\big)^{\frac{1}{2}}\mathbf{f}. \tag{3.85}$$

Thus, the covariance of $\mathbf{u}_1$ and $_2$ $cov(\mathbf{u}_1, \mathbf{u}_2)$ vanishes, and HI_j and E_j are independent. Consequently,

$$P\big(HI_j, E_j\big) = P\big(HI_j\big)P\big(E_j\big). \tag{3.86}$$

The Integrity and Continuity Risks

The general integrity and continuity risks a generic FDE method have been derived in [62]. To be more precise, the general integrity risk is

$$\begin{aligned} P_{IR} = &\sum_{i=0}^{n_{FH}} P(HI_0, ND|H_i)P(H_i) \\ &+ \sum_{i=0}^{n_{FH}}\sum_{j=1}^{n_{EH}} P(HI_j, D, E_j|H_i)P(H_i), \end{aligned} \tag{3.87}$$

and the general continuity risk is

$$\begin{aligned} P_{CR} = &P(D, NE|H_0)P(H_0) \\ &+ \sum_{i=1}^{n_{FH}} P(D, NE|H_i)P(H_i), \end{aligned} \tag{3.88}$$

In both (3.87) and (3.88), the notation $P\big(EVNT_1, EVNT_2|EVNT_3\big)$ denotes the conditional probability that $EVNT_1$ and $EVNT_2$ happen simultaneously, under the condition that $EVNT_3$ has happened. In other words, P_{IR} is the probability that the the vertical position error exceeds l_{al} when the FDE method claims that there's no faulty measurement or when the FDE method claims that all the faulty measurements are excluded, while P_{CR} is the probability that the generic FDE method claims that there are faulty measurements but is unable to exclude the faulty measurements. Both the P_{IR} and P_{CR} take into account the considered fault hypotheses.

3.3.2 An Integrity Risk Bound for the PQP approach

A way to verify the integrity of the PQP method for an application is to calculate the integrity risk P_{IR} and then to check if the calculated integrity risk is bounded from the above by the required integrity risk associated by the application. In this subsection, the PQP method is integrated with the integrity risk bound of the Chi-squared ARAIM derived in [62], and the integrity risk bound then allows for the verification of the integrity of the PQP method. Because ND implies $\overline{ND}$ and since HI_0 and $\overline{ND}$ are statically independent,

$$P\big(HI_0, ND|H_i\big) \leq P\big(HI_0|H_i\big)P\big(\overline{ND}|H_i\big), \tag{3.89}$$

for all considered fault hypotheses. Also,

$$P\big(HI_j, D, E_j|H_j\big) \leq P\big(HI_j, E_j|H_j\big) \tag{3.90}$$

As a result, an upper bound on P_{IR} is

$$\begin{aligned} P_{IRB} = &\sum_{i=0}^{n_{FH}} P(HI_0|H_i)P(\overline{ND}|H_i)P(H_i) \\ &+ \sum_{i=0}^{n_{FH}}\sum_{j=1}^{n_{EH}} P(HI_j|H_i)P(E_j|H_i)P(H_i). \end{aligned} \tag{3.91}$$

Before further simplifications of the P_{IRB} are pursuit, a few things are noted. While both $P(HI_0|H_i)$ and $P(HI_j|H_i)$ depend on l_{al}, $P(\overline{ND}|H_i)$ depends on h, and $P(E_j|H_i)$ depends on T_j^2. The value of l_{al} is given as a part of the integrity requirement, the parameter h can be tuned according to either the probability of false alarms or KDE, but it remains unclear how T_j^2 can be tuned.

The Determination of T_j^2

Similar to the integrity requirement, the continuity requirement is fulfilled if the P_{CR}, calculated according to (3.88), is bounded by the specified upper limit of continuity risk. Since $P\big(D, NE|H_0\big)$ is less than or equal to $P\big(D|H_0\big)$, which is just the probability of false alarms and should stay below some required upper limit $P_{FA,IRQ}$, and since $P\big(D, NE|H_i\big)$ does not exceed $P\big(NE|H_i\big)$, an upper bound for the continuity risk is

$$P_{CR} = P_{FA,REQ}P(H_0) + \sum_{i=1}^{n_{FH}} P(NE|H_i)P_{max}, \tag{3.92}$$

where

$$P_{max} = \max_{i\in\{1,\ldots,n_{FH}\}} P\big(H_i\big). \tag{3.93}$$

From (3.92), a naive way to determine the T_j^2 in (3.63) is

$$T_j^2 = \chi^{-2}\big(1 - \frac{P_{C,REQ} - P_{FA,REQ}P(H_0)}{P_{max}}, n_{sv} - m - n_j\big). \tag{3.94}$$

To be more precise, if the PQP method sets the j^{th} fault hypothesis as the candidate for exclusion, T_j^2 is the threshold used in the RAIM test in Figure 3.1. In (3.94), $\chi^{-2}(prob, \mu)$ represents the inverse cumulative distribution function of the Chi-squared distribution with *prob* probability and μ degrees of freedom, and n_j is the number of the candidates of faulty measurements assumed by the j^{th} fault hypothesis. A few remarks about the T_j^2 shown in (3.94). Firstly, the T_j^2 in (3.94) is naive because it uses P_{max} instead of the actual prior probability, say $P\big(H_j\big)$ for H_j, for each individual fault hypothesis. Also, the actual P_{CR} exceed P_{CRB} with the use of the T_j^2 in (3.94). A way to determine T_j^2 such that the P_{CR} does not exceed P_{CRB} is to consider the P_{CRB} as a budget to be distributed to the fault hypotheses [62]. That is, to find a set of non-negative coefficients β_i such that

$$\sum_{i=i}^{n_{FH}} \beta_i = 1, \tag{3.95}$$

and determine T_j^2 by

$$T_j^2 = \chi^{-2}\big(1 - \frac{P_{C,REQ} - P_{FA,REQ}P(H_0)}{\beta_i P_{max}}, n_{sv} - m - n_j\big). \tag{3.96}$$

The determination of the coefficients leads to interesting research topics but is out of the scope of this work. In this work, the T_j^2 in (3.94) is used.

The Worst Faults for the Fault Hypotheses

The P_{IRB} in (3.91) can be further simplified by finding the worst fault for each fault hypothesis, as derived and explained in [62]. Following the derivations, it is concluded that the worst fault that maximizes $P(HI_0|H_i)P(\overline{ND}|H_i)$ lies in the direction

$$\overline{\mathbf{f}}_{i,0} = \mathbf{A}_i\big(\mathbf{A}_i^T\mathbf{W}_{\frac{1}{2}}\mathbf{R}_0\mathbf{W}_{\frac{1}{2}}\mathbf{A}_i\big)^{-1}\mathbf{A}_i^T\mathbf{W}_{\frac{1}{2}}\mathbf{G}_0\mathbf{P}_0\boldsymbol{\alpha}. \tag{3.97}$$

Consequently, $P(HI_0|H_i)P(\overline{ND}|H_i)$ can be maximized by optimizing the magnitude of the fault vector along $\overline{\mathbf{f}}_{i,0}$. Similarly, the worst fault that maximizes $P(HI_j|H_i)P(E_j|H_i)$ lies in the direction

$$\overline{\mathbf{f}}_{i,j} = \mathbf{A}_i\big(\mathbf{A}_i^T\mathbf{W}_{\frac{1}{2}}\mathbf{B}_j\mathbf{R}_j\mathbf{B}_j^T\mathbf{W}_{\frac{1}{2}}\mathbf{A}_i\big)^{-1}\mathbf{A}_i^T\mathbf{W}_{\frac{1}{2}}\mathbf{B}_j\mathbf{G}_j\mathbf{P}_j\boldsymbol{\alpha}, \tag{3.98}$$

and $P(HI_j|H_i)P(E_j|H_i)$ can be maximized by finding the magnitude of the fault vector along $\overline{\mathbf{f}}_{i,j}$. Writing the found magnitudes $\omega_{i,0}$ and $\omega_{i,j}$ of $P(HI_j|H_i)P(E_j|H_i)$ and $P(HI_j|H_i)P(E_j|H_i)$, respectively. The P_{IRB} in (3.91) becomes

$$P_{IRB} = \sum_{i=0}^{n_{FH}} P(HI_0|\mathbf{f} = \omega_{i,0}\mathbf{f}_{i,0})P(\overline{ND}|\mathbf{f} = \omega_{i,0}\mathbf{f}_{i,0})P(H_i) + \sum_{i=0}^{n_{FH}} \sum_{j=1}^{n_{EH}} P(HI_j|\mathbf{f} = \omega_{i,j}\mathbf{f}_{i,j})P(E_j|\mathbf{f} = \omega_{i,j}\mathbf{f}_{i,j})P(H_i). \tag{3.99}$$

The proofs of the worst faults (3.97) and (3.97) follow from those shown in [62,80], and are outlined here. As reported in [80, 81], it is necessary that the worst fault $\overline{\mathbf{f}}_{i,0}$ maximizes the ratio

$$s_{i,0}(\mathbf{f}) = \frac{{\mu_{\mathbf{v},\mathbf{1}}}^T \mu_{\mathbf{v},\mathbf{1}}}{{\mu_{\mathbf{v},\mathbf{2}}}^T \mu_{\mathbf{v},\mathbf{2}}} = \frac{\mathbf{f}^T \mathbf{N}_v \mathbf{f}}{\mathbf{f}^T \mathbf{D}_v \mathbf{f}}. \tag{3.100}$$

where

$$\mathbf{N}_v = \mathbf{n}_v^T \mathbf{n}_v, \tag{3.101}$$

$$\mathbf{n}_v = \boldsymbol{\alpha}_v^T \mathbf{P}_0 \mathbf{G}_0^T \mathbf{W}_{\frac{1}{2}}, \tag{3.102}$$

and

$$\mathbf{D}_v = \mathbf{W}_{\frac{1}{2}} \mathbf{Q}^T \mathbf{Q} \mathbf{W}_{\frac{1}{2}} = \mathbf{W}_{\frac{1}{2}} \mathbf{R}_0 \mathbf{W}_{\frac{1}{2}}. \tag{3.103}$$

Now, consider the change of variables

$$\mathbf{D}_{v,\frac{1}{2}} \mathbf{A}_i \widetilde{\mathbf{f}} = \mathbf{f}, \tag{3.104}$$

Since $\mathbf{A}^T \mathbf{D}_v \mathbf{A}$ is symmetric and positive definite, it can be factored into $\mathbf{D}_{\mathbf{A},v,\frac{1}{2}} \mathbf{D}_{\mathbf{A},v,\frac{1}{2}}$, where $\mathbf{D}_{\mathbf{A},v,\frac{1}{2}}$ is the positive square root of $\mathbf{A}^T \mathbf{D}_v \mathbf{A}$. Now consider another change of variables

$$\overline{\widetilde{\mathbf{f}}} = \mathbf{D}_{v,\frac{1}{2}} \mathbf{A}_i \widetilde{\mathbf{f}}, \tag{3.105}$$

and denote $\left(\mathbf{D}_{v,\frac{1}{2}}\right)^{-1}\mathbf{A}_i$ by $\mathbf{D}^{-1}_{A,v,\frac{1}{2}}$, $s_{i,0}(\mathbf{f})$ becomes

$$s_{i,0}(\bar{\bar{\mathbf{f}}}) = \frac{\bar{\bar{\mathbf{f}}}^T(\mathbf{D}^{-1}_{\mathbf{A},v,\frac{1}{2}})^T(\mathbf{A}_i^T\mathbf{N}_v\mathbf{A}_i)(\mathbf{D}^{-1}_{\mathbf{A},v,\frac{1}{2}})\bar{\bar{\mathbf{f}}}}{\bar{\bar{\mathbf{f}}}^T\bar{\bar{\mathbf{f}}}}. \tag{3.106}$$

Let

$$\begin{aligned}\mathbf{M}_s &= (\mathbf{D}^{-1}_{\mathbf{A},v,\frac{1}{2}})^T(\mathbf{A}_i^T\mathbf{N}_v\mathbf{A}_i)(\mathbf{D}^{-1}_{\mathbf{A},v,\frac{1}{2}}) \\ &= (\mathbf{D}^{-1}_{\mathbf{A},v,\frac{1}{2}})^T(\mathbf{n}_v\mathbf{A}_i)^T(\mathbf{n}_v\mathbf{A}_i)(\mathbf{D}^{-1}_{\mathbf{A},v,\frac{1}{2}})\end{aligned} \tag{3.107}$$

and notice that $\mathbf{M}_s$ is symmetric, it follows from the spectral theorem that $\mathbb{R}^{n_i}$, where n_i is the number of faulty measurements assumed by the i^{th} fault hypothesis, admits an orthonormal basis consisting the eigenvector of $\mathbf{M}_s$ [58], which in turn shows that $s_{i,0}(\bar{\bar{\mathbf{f}}})$ can be maximized over the set of nonzero $\bar{\bar{\mathbf{f}}}$ that belongs to $\mathbb{R}^{n_i}$. To be more precise

$$\max_{\bar{\bar{\mathbf{f}}}\neq\mathbf{0}} s_{i,0}(\bar{\bar{\mathbf{f}}}) = \max_{\bar{\bar{\mathbf{f}}}\neq\mathbf{0}} \frac{\bar{\bar{\mathbf{f}}}^T\mathbf{M}_s\bar{\bar{\mathbf{f}}}}{\bar{\bar{\mathbf{f}}}^T\bar{\bar{\mathbf{f}}}} = \lambda_{max}, \tag{3.108}$$

where λ_{max} is the largest eigenvalue of $\mathbf{M}_s$, and λ_{max} can be attained by the eigenvector corresponding to λ_{max}. From (3.107), the singular value decomposition of $\mathbf{M}_s$ is

$$\mathbf{M}_s = \frac{(\mathbf{D}^{-1}_{\mathbf{A},v,\frac{1}{2}})^T(\mathbf{n}_v\mathbf{A}_i)^T}{\|(\mathbf{n}_v\mathbf{A}_i)(\mathbf{D}^{-1}_{\mathbf{A},v,\frac{1}{2}})\|_2}\left(\|(\mathbf{n}_v\mathbf{A}_i)(\mathbf{D}^{-1}_{\mathbf{A},v,\frac{1}{2}})\|_2\right)^2\frac{(\mathbf{n}_v\mathbf{A}_i)(\mathbf{D}^{-1}_{\mathbf{A},v,\frac{1}{2}})}{\|(\mathbf{n}_v\mathbf{A}_i)(\mathbf{D}^{-1}_{\mathbf{A},v,\frac{1}{2}})\|_2}, \tag{3.109}$$

and it shows that $\mathbf{M}_s$ has only one nonzero eigenvalue and

$$(\mathbf{D}^{-1}_{\mathbf{A},v,\frac{1}{2}})^T(\mathbf{n}_v\mathbf{A}_i)^T \tag{3.110}$$

is an eigenvector in $\mathbb{R}^{n_i}$ that corresponds to the eigenvalue λ_{max}. In $\mathbb{R}^{n_{sv}}$, the direction of the eigenvector shown by (3.110) is

$$\mathbf{A}_i(\mathbf{D}^{-1}_{\mathbf{A},v,\frac{1}{2}})(\mathbf{D}^{-1}_{\mathbf{A},v,\frac{1}{2}})^T(\mathbf{n}_v\mathbf{A}_i)^T = (\mathbf{A}_i)(\mathbf{A}_i^T\mathbf{D}_v\mathbf{A}_i)^{-1}(\mathbf{A}_i)^T(\mathbf{n}_v)^T. \tag{3.111}$$

Upon substitutions of $\mathbf{n}_v$ and $\mathbf{D}_v$ by (3.102) and (3.103) respectively, the $\overline{\mathbf{f}}_{i,0}$ in (3.97) results.

For the proof for the $\overline{\mathbf{f}}_{i,j}$ in (3.98), consider

$$s_{i,j}(\mathbf{f}) = \frac{{\mu_{\mathbf{u},\mathbf{1}}}^T\mu_{\mathbf{u},\mathbf{1}}}{{\mu_{\mathbf{u},\mathbf{2}}}^T\mu_{\mathbf{u},\mathbf{2}}} = \frac{\mathbf{f}^T\mathbf{N}_u\mathbf{f}}{\mathbf{f}^T\mathbf{D}_u\mathbf{f}}. \tag{3.112}$$

In (3.112),

$$\mathbf{N}_u = \mathbf{n}_u^T\mathbf{n}_u, \tag{3.113}$$

$$\mathbf{n}_u = \boldsymbol{\alpha}_v^T\mathbf{P}_j\mathbf{G}_j^T\mathbf{B}_j\mathbf{W}_{\frac{1}{2}}, \tag{3.114}$$

and

$$\begin{aligned}\mathbf{D}_u &= \mathbf{B}_{j,\frac{1}{2}}\mathbf{R}_j\mathbf{B}^T_{j,\frac{1}{2}} \\ &= \mathbf{W}_{\frac{1}{2}}\mathbf{B}_j\mathbf{R}_j\mathbf{B}_j^T\mathbf{W}_{\frac{1}{2}}\end{aligned}. \tag{3.115}$$

Using the change of variables

$$\mathbf{D}_{u,\frac{1}{2}}\mathbf{A}_i\widetilde{\mathbf{f}} = \mathbf{f}, \tag{3.116}$$

where $\mathbf{D}_{u,\frac{1}{2}}$ is the positive square root of $\mathbf{D}_u$ then

$$s_{i,j}(\widetilde{\mathbf{f}}) = \frac{\widetilde{\mathbf{f}}^T\mathbf{A}_i^T\mathbf{N}_u\mathbf{A}_i\widetilde{\mathbf{f}}}{\widetilde{\mathbf{f}}^T\mathbf{A}_i^T\mathbf{D}_u\mathbf{A}_i\widetilde{\mathbf{f}}}. \tag{3.117}$$

Now, consider a second change of variables

$$\overline{\widetilde{\mathbf{f}}} = \mathbf{D}_{u,\frac{1}{2}}\mathbf{A}_i\widetilde{\mathbf{f}}, \tag{3.118}$$

where $\mathbf{D}_{u,\frac{1}{2}}$ is the positive square root of $\mathbf{D}_u$. If $\left(\mathbf{D}_{u,\frac{1}{2}}\right)^{-1}\mathbf{A}_i$ is denoted by $\mathbf{D}^{-1}_{A,u,\frac{1}{2}}$, then

$$s_{i,j}(\bar{\bar{\mathbf{f}}}) = \frac{\bar{\bar{\mathbf{f}}}^T(\mathbf{D}^{-1}_{\mathbf{A},u,\frac{1}{2}})^T(\mathbf{A}_i^T\mathbf{N}_u\mathbf{A}_i)(\mathbf{D}^{-1}_{\mathbf{A},u,\frac{1}{2}})\bar{\bar{\mathbf{f}}}}{\bar{\bar{\mathbf{f}}}^T\bar{\bar{\mathbf{f}}}}. \tag{3.119}$$

From the discussion for if follows that worst fault direction $\bar{\mathbf{f}}_{i,j}$ is

$$\mathbf{A}_i(\mathbf{D}^{-1}_{\mathbf{A},u,\frac{1}{2}})(\mathbf{D}^{-1}_{\mathbf{A},u,\frac{1}{2}})^T(\mathbf{n}_u\mathbf{A}_i)^T = (\mathbf{A}_i)(\mathbf{A}_i^T\mathbf{D}_u\mathbf{A}_i)^{-1}(\mathbf{A}_i)^T(\mathbf{n}_u)^T, \tag{3.120}$$

which is equal to the one shown in (3.98).

3.3.3 Vertical Protection Level Calculations for the PQP Approach

In addition to calculating the integrity risk bounds and then comparing them to the required integrity risk, vertical protection levels facilitate a different way to verify the integrity of FDE for vertical navigation. Simply put, vertical protection levels can be calculated from the integrity risk bounds and then compared with the required alert limit. In subsection, it is demonstrated that a vertical protection level can be calculated from the P_{IRB} in (3.91). In particular, it will be shown how upper and lower bounds of vertical protection levels can be calculated using the method proposed in [82].

The Vertical Protection Level for Detection and Exclusion Using the PQP Method

Instead of calculating P_{IRB} in (3.91) and then comparing the result with $P_{IR,REQ}$, the alert limit l_{AL} is first considered as a variable l and the integrity risk bound is regarded as a function of l, which is denoted by $P_{IRB}(l)$. The $P_{IRB}(l)$ is then equated with $P_{IR,REQ}$ and solved for the solution, which is denoted by l_{PL}. Finally, l_{PL} is compared with l_{AL}. The integrity risk requirement is satisfied if l_{PL} is not greater

than l_{AL}. For the purpose of illustration, $P(HI_0|H_i)$, $P(HI_j|H_i)$, $P(\overline{ND}|H_i)P(H_i)$, and $P(E_j|H_i)P(H_i)$ are denoted by

$$P(HI_0|H_i) = P_{HI_{0,i}}(l), \tag{3.121}$$

$$P(HI_j|H_i) = P_{HI_{j,i}}(l), \tag{3.122}$$

$$P(\overline{ND}|H_i)P(H_i) = c_{0i}, \tag{3.123}$$

and

$$P(E_j|H_i)P(H_i) = c_{ji}. \tag{3.124}$$

Now, calculating l_{PL} is equivalent to solving for the l_{PL} from

$$\sum_{i=0}^{n_{FH}} c_{0,i} P_{HI_{0,i}}(l_{PL}) + \sum_{j=1}^{n_{EH}} \sum_{i=0}^{n_{FH}} c_{j,i} P_{HI_{j,i}}(l_{PL}) = P_{IR,REQ}. \tag{3.125}$$

One of the most commonly used methods to solve (3.125) is to consider $P_{IR,REQ}$ as a budget to be distributed to $P_{HI_0}(l)$ and $P_{HI_j}(l)$ in (3.125) [82]. That is, we formulate the l_{PL} calculation into the optimization problem

$$l_{PL} = \max\{l_{j,i}\}, \tag{3.126}$$

$$c_{j,i} P_{HI_j}(l_{j,i}) = \alpha_{j,i} P_{IR,REQ}, \tag{3.127}$$

$$0 < \alpha_{j,i} < 1, \tag{3.128}$$

and

$$\sum_{j=1}^{n_{EH}} \sum_{i=0}^{n_{FH}} \alpha_{j,i} = 1, \tag{3.129}$$

for all $i \in \{0, \ldots, n_{FH}\}$ and $j \in \{1, \ldots, n_{FH}\}$.

The Vertical Protection Level for Detection Using the PQP Method

In this subsection, the vertical protection level calculation of the solution separation ARAIM proposed in [82] is briefly described. In particular, it is explained the how the associated lower and upper bounds derived in [82] can be used to calculate a lower bound and an upper bound for the l_{PL} of PQP method. For detection only, the P_{HMI} in (3.91) reduces to

$$P_{IRB} = \sum_{i=0}^{n_{FH}} P(HI_0, ND|H_i)P(H_i). \tag{3.130}$$

Similar to the calculation of right hand side terms in (3.129), the calculation of P_{IRB} in (3.130) takes l_{AL}, T_0, and all T_i as its input parameters. Again, the l_{AL} in (3.130) is replaced with a variable l and P_{HMI} is considered as a function of l, $P_{HMI}(l)$. Calculating l_{PL} amounts to solving

$$P_{HMI}(l_{PL}) = P_{IR,REQ}, \tag{3.131}$$

for l_{PL}. In [82], a l_{PL} and the associated lower and upper bounds are proposed. The first step to calculate l_{PL} using the simplified calculation is to check if

$$p^T p \leq T_0. \tag{3.132}$$

The detection threshold T_0 is determined by

$$T_0 = \chi^{-2}(1 - P_{FA,REQ}, n_{sv} - m), \tag{3.133}$$

where $\chi^{-2}(1 - P_{FA,REQ}, n_{sv} - m)$ is the inverse cumulative distribution function of the central Chi-squared distribution with $n_{sv} - m$ degrees of freedom and the probability $1 - P_{FA,REQ}$. If (3.132) is true, the next step is to calculate for each H_i, $i \in \{1, \ldots, n_{FH}\}$,

$$T_i = \sigma_{ss,i}\sqrt{T_0}. \tag{3.134}$$

In (3.134),

$$\sigma_{ss,i} = \alpha^T (S_i - S_0)(S_i - S_0)^T \alpha, \tag{3.135}$$

where

$$S_0 = P_0 G_0 W_{\frac{1}{2}}, \tag{3.136}$$

and

$$S_i = P_i G_i W_{\frac{1}{2}}. \tag{3.137}$$

Also calculated for each H_i is

$$\sigma_i = \sqrt{\alpha^T P_i \alpha}. \tag{3.138}$$

The l_{PL} can be solved using a half interval search, and a lower bound $l_{PL,LB}$ and an upper bound $l_{PL,UB}$ can also be calculated [82]. The calculations of $l_{PL,LB}$ and $l_{PL,UB}$ start with

$$l_{PL,low,init} = \max\{Q^{-1}(v_{l,0})\sigma_0, \max\{Q^{-1}(v_{l,i})\sigma_i + T_i\}\}, \tag{3.139}$$

and

$$l_{PL,up,init} = \max\{Q^{-1}(v_{u,0})\sigma_0, \max\{Q^{-1}(v_{u,i})\sigma_i + T_i\}\}, \tag{3.140}$$

where $Q^{-1}(p)$ denotes the $(1-p)$-quantile of the standard normal distribution. Also, $v_{l,0}$ equals $\frac{P_{IR,REQ}}{2}$, $v_{l,i}$ equals $\frac{P_{IR,REQ}}{P(H_i)}$, $v_{u,0}$ equals $\frac{P_{IR,REQ}}{2(n_{FH}+1)}$, and $v_{u,i}$ equals $\frac{P_{IR,REQ}}{P(H_i)(n_{FH}+1)}$. From (3.139) and (3.140), we can calculate a lower bound and an upper bound by

$$\begin{aligned} l_{PL,LB} =& l_{PL,low,init} \\ &+ \left(\left(P_{IR,REQ} - P_{exceed}(l_{PL,low,init}) \right) \right. \\ &\left. \times \frac{l_{PL,up,init} - l_{PL,low,init}}{P_{exceed}(l_{PL,up,init}) - P_{exceed}(l_{PL,low,init})} \right), \end{aligned} \tag{3.141}$$

and

$$\begin{aligned} l_{PL,UB} =& l_{PL,up,init} \\ &+ \Bigg(\Big(log\big(P_{IR,REQ}\big) - log\big(P_{exceed}(l_{PL,low,init})\big) \Big) \\ &\times \frac{l_{PL,up,init} - l_{PL,low,init}}{P_{exceed}(l_{PL,up,init}) - P_{exceed}(l_{PL,low,init})} \Bigg), \end{aligned} \tag{3.142}$$

respectively. In (3.141) and (3.142)

$$P_{exceed}(l) = 2Q\bigg(\frac{l}{\sigma_0}\bigg) + \sum_{i=1}^{n_{FH}} P(H_i) Q\bigg(\frac{l - T_i}{\sigma i}\bigg), \tag{3.143}$$

where $Q(l)$ is the tail probability of the zero mean unit variance normal distribution [83], evaluated at l.

In order to calculate $l_{PL,LB}$ and $l_{PL,UB}$ for fault detection using the PQP method by (3.141) and (3.142), two changes are made. The first change is related to (3.132). Instead of checking if (3.132) is true, we check if $\hat{f}$ is the zero vector. The calculated $l_{PL,LB}$ and $l_{PL,UB}$ are valid only if $\hat{f}$ is the zero vector. The second change is to replace T_0 in (3.133) and (3.134) by

$$T_0 = n_{sv} h^2. \tag{3.144}$$

The idea behind these two changes is that if the $\hat{f}$ is the zero vector, then the received measurement will pass the solution separation test in [82] with the T_0 equal to $n_{sv}h^2$ and all T_i equal to $\sigma_{ss,i} h \sqrt{n_{sv}}$. In this case, we can calculate the corresponding $l_{PL,LB}$ and $l_{PL,UB}$ using (3.141) and (3.142).

Using the KDE Parameter Tuning Method

Tuning the PQP parameter, h, according to (3.27) guarantees that the probability of false alarm will not exceed $P_{FA,REQ}$ [52]. Such PQP parameter is not optimal in

the sense that it does not result in tight vertical protection level and the associated bounds, given the probability of false alarm is no more than $P_{FA,REQ}$. The crux of this problem is that it is unclear how the PQP detection statistic, $\|Q^T p\|_\infty$, distributes analytically under the fault-free hypothesis, H_0. Fortunately, the fault vector in (2.17) vanishes under H_0. In this case, it is possible to simulate samples of $\|Q^T p\|_\infty$ using (2.17) and (2.23). Then, the cumulative distribution function can be estimated using the simulated samples and a selected kernel function [44, 84, 85]. Denoting the resulting estimate of the cumulative distribution function by CDF_{KDE}, h can be tuned according to

$$h_{KDE} = CDF_{KDE}^{-1}(1 - P_{FA,REQ}), \tag{3.145}$$

where $CDF_{KDE}^{-1}(1 - P_{FA,REQ})$ is the inverse of CDF_{KDE} evaluated at $1 - P_{FA,REQ}$. The h obtained from (3.145) is less conservative and results in lower vertical protection level and $l_{PL,LB}$ and $l_{PL,UB}$. A final remark about the h obtained from (3.145) is that, unlike the h tuned according to (3.27), the probability of false alarm may exceed $P_{FA,REQ}$. [86].

4. NUMERICAL EXAMPLES

In this chapter, numerical examples, which include the FDE using the PQP method, the integrity risk bound of the PQP method, and both the lower and upper bounds of the vertical protection level in the case of detection, are presented. The examples are taken from a paper that has been accepted for publication [52] and a paper that is currently under review [86].

The software tools used to generate the numerical examples are developed using the Qt Creator [87] , the Eigen C++ template library [88] , the boost C++ libraries [89, 90] , and the gurobi optimization library [91] .

The satellite measurements used in the examples come from the GPS, GLONASS, and Beidou satellites, all of which are extracted from a GNSS receiver that is connected to a antenna at a fixed and known location. The line-of-sight (LOS) direction vectors are obtained using the satellites and user positions, which are contained in the receiver output. The LOS direction vectors are summarized in Table 4.1, Table 4.2, and Table 4.3, respectively. The values in Table 4.1, Table 4.2, and Table 4.3 are used to construct the tested satellite geometries summarized in Table 4.4. Suppose for now that $\mathbf{G}_{two}$ is the geometry matrix for satellite geometry 2, then $\mathbf{G}_{two}$ is a 12×4 matrix that takes the following form

$$\mathbf{G}_{two} = \begin{bmatrix} \vdots & \vdots & \vdots & \vdots \\ E_i & N_i & U_i & 1 \\ \vdots & \vdots & \vdots & \vdots \end{bmatrix}. \tag{4.1}$$

Table 4.1. Line-of-Sight components of the GPS Satellites

Constellation	Line-of-Sight components		
	E	N	U
GPS	8.5334×10^{-1}	-2.1582×10^{-3}	-5.1807×10^{-1}
GPS	3.7866×10^{-1}	8.6053×10^{-1}	-3.4119×10^{-1}
GPS	$-.2.1614 \times 10^{-1}$	3.9521×10^{-1}	-8.9280×10^{-1}
GPS	3.5034×10^{-1}	-1.7313×10^{-1}	-9.2048×10^{-1}
GPS	-9.0776×10^{-1}	1.5131×10^{-1}	-3.9125×10^{-1}
GPS	7.7386×10^{-1}	3.4472×10^{-1}	-5.3134×10^{-1}
GPS	5.4021×10^{-1}	-6.0939×10^{-1}	-5.8037×10^{-1}
GPS	-3.0590×10^{-3}	-4.3559×10^{-1}	-9.0014×10^{-1}
GPS	7.6416×10^{-2}	6.40192×10^{-1}	-7.6441×10^{-1}
GPS	-5.7118×10^{-1}	-7.0984×10^{-1}	-4.1216×10^{-1}
GPS	-5.0147×10^{-1}	-2.9867×10^{-1}	-8.1199×10^{-1}
GPS	-3.8672×10^{-1}	6.9339×10^{-1}	-6.0800×10^{-1}

Table 4.2. Line-of-Sight components of the GLONASS Satellites

Constellation	Line-of-Sight components		
	E	N	U
GLONASS	2.5858×10^{-1}	6.8390×10^{-1}	-6.8222×10^{-1}
GLONASS	-6.6621×10^{-1}	-5.2417×10^{-1}	-5.3049×10^{-1}
GLONASS	-9.9014×10^{-2}	-6.7353×10^{-1}	-7.3250×10^{-1}
GLONASS	7.3723×10^{-1}	-4.2378×10^{-1}	-5.2622×10^{-1}
GLONASS	-6.1703×10^{-1}	1.1442×10^{-1}	-7.7858×10^{-1}
GLONASS	-3.0099×10^{-1}	7.5154×10^{-1}	-5.8702×10^{-1}
GLONASS	-6.0027×10^{-1}	-5.7338×10^{-1}	-5.5759×10^{-1}

Table 4.3. Line-of-Sight components of the Beidou Satellites

Constellation	Line-of-Sight components		
	E	N	U
Beidou	-3.3759×10^{-1}	3.5243×10^{-1}	-8.7283×10^{-1}
Beidou	5.9029×10^{-1}	3.4358×10^{-1}	-7.3042×10^{-1}
Beidou	1.6708×10^{-1}	3.8715×10^{-1}	-9.0675×10^{-1}
Beidou	-6.4008×10^{-1}	2.9773×10^{-1}	-7.0828×10^{-1}
Beidou	8.7910×10^{-1}	2.0743×10^{-1}	-4.2913×10^{-1}
Beidou	9.0053×10^{-2}	4.7952×10^{-1}	-8.7290×10^{-1}
Beidou	1.3906×10^{-1}	-4.3905×10^{-1}	-8.8764×10^{-1}
Beidou	-2.4136×10^{-1}	8.7690×10^{-1}	-4.1568×10^{-1}
Beidou	3.0684×10^{-1}	1.06955×10^{-1}	-9.4573×10^{-1}
Beidou	5.3570×10^{-1}	-2.8382×10^{-1}	-7.9528×10^{-1}
Beidou	-2.6773×10^{-1}	5.3405×10^{-1}	-8.0194×10^{-1}
Beidou	1.1111×10^{-1}	9.6186×10^{-1}	-2.4997×10^{-1}

In (4.1), E_i, N_i, and U_i are the E, N, and U components of the i^{th} row of Table 4.1. The geometry matrix for satellite geometry 1 can be similarly constructed by using only the first eight satellites in Table 4.1. To construct the geometry matrix $\mathbf{G}_{three}$ for satellite geometry 3, let's suppose $\mathbf{G}_{T2}$ is the geometry for constructed using all and only all the satellites shown in Table 4.2. Note that $\mathbf{G}_{T2}$ is thus a 7×4 matrix. Now we can partition $\mathbf{G}_{T1}$ and $\mathbf{G}_{T2}$ according to

$$\mathbf{G}_{T1} = \begin{bmatrix} \mathbf{G}_{s1} & \mathbf{1}_{s1} \end{bmatrix}, \tag{4.2}$$

and

$$\mathbf{G}_{T2} = \begin{bmatrix} \mathbf{G}_{s2} & \mathbf{1}_{s2} \end{bmatrix}. \tag{4.3}$$

In (4.2) and (4.3), $\mathbf{1}_{s1}$ and $\mathbf{1}_{s2}$ are column vectors whose components are all ones and both $\mathbf{1}_{s1}$ and $\mathbf{1}_{s2}$ are of the appropriate dimensions. Also $\mathbf{G}_{s1}$ and $\mathbf{G}_{s2}$ are the submatrices that fit into the partitions. Now, the geometry matrix for satellite geometry 3 can be written as

Table 4.4. Satellite Geometries

Satellite Geometry	n_{sv}	Discription
1	8	first 8 GPS satellites
2	12	all GPS satellites
3	19	all GPS and GLONASS satellites
4	24	all GPS and Beidou satellites
5	31	all GPS, GLONASS, and Beidou satellites

$$\mathbf{G}_{three} = \begin{bmatrix} \mathbf{G}_{s1} & \mathbf{1}_{s1} & \mathbf{0}_{s1} \\ \mathbf{G}_{s2} & \mathbf{0}_{s2} & \mathbf{1}_{s2} \end{bmatrix}, \tag{4.4}$$

where $\mathbf{0}_{s1}$ and $\mathbf{0}_{s2}$ are the respective zero vectors of the appropriate dimensions. If the geometry matrix for the satellites in Table 4.3 is

$$\mathbf{G}_{T3} = \begin{bmatrix} \mathbf{G}_{s3} & \mathbf{1}_{s3} \end{bmatrix}, \tag{4.5}$$

then the geometry matrix for satellite geometry 5 is

$$\mathbf{G}_{five} = \begin{bmatrix} \mathbf{G}_{s1} & \mathbf{1}_{s1} & \mathbf{0}_{s1} & \mathbf{0}_{s1} \\ \mathbf{G}_{s2} & \mathbf{0}_{s2} & \mathbf{1}_{s2} & \mathbf{0}_{s2} \\ \mathbf{G}_{s3} & \mathbf{0}_{s3} & \mathbf{0}_{s3} & \mathbf{1}_{s3} \end{bmatrix}. \tag{4.6}$$

Once again, $\mathbf{0}_{s3}$ is the zero vector of the appropriate dimensions To be more precise, the geometry matrix for satellite geometry 1 is

$$\mathbf{G}_{one} = \begin{bmatrix} 8.5334 \times 10^{-1} & -2.1582 \times 10^{-3} & -5.1807 \times 10^{-1} & 1.0 \\ 3.7866 \times 10^{-1} & 8.6053 \times 10^{-1} & -3.4119 \times 10^{-1} & 1.0 \\ -2.1614 \times 10^{-1} & 3.9521 \times 10^{-1} & -8.9280 \times 10^{-1} & 1.0 \\ 3.5034 \times 10^{-1} & -1.7313 \times 10^{-1} & -9.2048 \times 10^{-1} & 1.0 \\ -9.0776 \times 10^{-1} & 1.5131 \times 10^{-1} & -3.9125 \times 10^{-1} & 1.0 \\ 7.7386 \times 10^{-1} & 3.4472 \times 10^{-1} & -5.3134 \times 10^{-1} & 1.0 \\ 5.4021 \times 10^{-1} & -6.0939 \times 10^{-1} & -5.8037 \times 10^{-1} & 1.0 \\ -3.0590 \times 10^{-3} & -4.3559 \times 10^{-1} & -9.0014 \times 10^{-1} & 1.0 \end{bmatrix}. \tag{4.7}$$

The geometry matrix for satellite geometry 2 is

$$\mathbf{G}_{two} = \begin{bmatrix} 8.5334 \times 10^{-1} & -2.1582 \times 10^{-3} & -5.1807 \times 10^{-1} & 1.0 \\ 3.7866 \times 10^{-1} & 8.6053 \times 10^{-1} & -3.4119 \times 10^{-1} & 1.0 \\ -2.1614 \times 10^{-1} & 3.9521 \times 10^{-1} & -8.9280 \times 10^{-1} & 1.0 \\ 3.5034 \times 10^{-1} & -1.7313 \times 10^{-1} & -9.2048 \times 10^{-1} & 1.0 \\ -9.0776 \times 10^{-1} & 1.5131 \times 10^{-1} & -3.9125 \times 10^{-1} & 1.0 \\ 7.7386 \times 10^{-1} & 3.4472 \times 10^{-1} & -5.3134 \times 10^{-1} & 1.0 \\ 5.4021 \times 10^{-1} & -6.0939 \times 10^{-1} & -5.8037 \times 10^{-1} & 1.0 \\ -3.0590 \times 10^{-3} & -4.3559 \times 10^{-1} & -9.0014 \times 10^{-1} & 1.0 \\ 7.6416 \times 10^{-2} & 6.4019 \times 10^{-1} & -7.6441 \times 10^{-1} & 1.0 \\ -5.7118 \times 10^{-1} & -7.0984 \times 10^{-1} & -4.1216 \times 10^{-1} & 1.0 \\ -5.0147 \times 10^{-1} & -2.9867 \times 10^{-1} & -8.1199 \times 10^{-1} & 1.0 \\ -3.8672 \times 10^{-1} & 6.9339 \times 10^{-1} & -6.0800 \times 10^{-1} & 1.0 \end{bmatrix}. \tag{4.8}$$

The geometry matrix for satellite geometry 3 is

$$\mathbf{G}_{three} = \begin{bmatrix} 8.5334 \times 10^{-1} & -2.1582 \times 10^{-3} & -5.1807 \times 10^{-1} & 1.0 & 0.0 \\ 3.7866 \times 10^{-1} & 8.6053 \times 10^{-1} & -3.4119 \times 10^{-1} & 1.0 & 0.0 \\ -2.1614 \times 10^{-1} & 3.9521 \times 10^{-1} & -8.9280 \times 10^{-1} & 1.0 & 0.0 \\ 3.5034 \times 10^{-1} & -1.7313 \times 10^{-1} & -9.2048 \times 10^{-1} & 1.0 & 0.0 \\ -9.0776 \times 10^{-1} & 1.5131 \times 10^{-1} & -3.9125 \times 10^{-1} & 1.0 & 0.0 \\ 7.7386 \times 10^{-1} & 3.4472 \times 10^{-1} & -5.3134 \times 10^{-1} & 1.0 & 0.0 \\ 5.4021 \times 10^{-1} & -6.0939 \times 10^{-1} & -5.8037 \times 10^{-1} & 1.0 & 0.0 \\ -3.0590 \times 10^{-3} & -4.3559 \times 10^{-1} & -9.0014 \times 10^{-1} & 1.0 & 0.0 \\ 7.6416 \times 10^{-2} & 6.4019 \times 10^{-1} & -7.6441 \times 10^{-1} & 1.0 & 0.0 \\ -5.7118 \times 10^{-1} & -7.0984 \times 10^{-1} & -4.1216 \times 10^{-1} & 1.0 & 0.0 \\ -5.0147 \times 10^{-1} & -2.9867 \times 10^{-1} & -8.1199 \times 10^{-1} & 1.0 & 0.0 \\ -3.8672 \times 10^{-1} & 6.9339 \times 10^{-1} & -6.0800 \times 10^{-1} & 1.0 & 0.0 \\ 2.5858 \times 10^{-1} & 6.8390 \times 10^{-1} & -6.8222 \times 10^{-1} & 0.0 & 1.0 \\ -6.6621 \times 10^{-1} & -5.2417 \times 10^{-1} & -5.3049 \times 10^{-1} & 0.0 & 1.0 \\ -9.9014 \times 10^{-2} & -6.7353 \times 10^{-1} & -7.3250 \times 10^{-1} & 0.0 & 1.0 \\ 7.3723 \times 10^{-1} & -4.2378 \times 10^{-1} & -5.2622 \times 10^{-1} & 0.0 & 1.0 \\ -6.1703 \times 10^{-1} & 1.1442 \times 10^{-1} & -7.7858 \times 10^{-1} & 0.0 & 1.0 \\ -3.0099 \times 10^{-1} & 7.5154 \times 10^{-1} & -5.8702 \times 10^{-1} & 0.0 & 1.0 \\ -6.0027 \times 10^{-1} & -5.7338 \times 10^{-1} & -5.5759 \times 10^{-1} & 0.0 & 1.0 \end{bmatrix}. \quad (4.9)$$

The geometry matrix for satellite geometry 4 is

$$\mathbf{G}_{four} = \begin{bmatrix} 8.5334 \times 10^{-1} & -2.1582 \times 10^{-3} & -5.1807 \times 10^{-1} & 1.0 & 0.0 \\ 3.7866 \times 10^{-1} & 8.6053 \times 10^{-1} & -3.4119 \times 10^{-1} & 1.0 & 0.0 \\ -2.1614 \times 10^{-1} & 3.9521 \times 10^{-1} & -8.9280 \times 10^{-1} & 1.0 & 0.0 \\ 3.5034 \times 10^{-1} & -1.7313 \times 10^{-1} & -9.2048 \times 10^{-1} & 1.0 & 0.0 \\ -9.0776 \times 10^{-1} & 1.5131 \times 10^{-1} & -3.9125 \times 10^{-1} & 1.0 & 0.0 \\ 7.7386 \times 10^{-1} & 3.4472 \times 10^{-1} & -5.3134 \times 10^{-1} & 1.0 & 0.0 \\ 5.4021 \times 10^{-1} & -6.0939 \times 10^{-1} & -5.8037 \times 10^{-1} & 1.0 & 0.0 \\ -3.0590 \times 10^{-3} & -4.3559 \times 10^{-1} & -9.0014 \times 10^{-1} & 1.0 & 0.0 \\ 7.6416 \times 10^{-2} & 6.4019 \times 10^{-1} & -7.6441 \times 10^{-1} & 1.0 & 0.0 \\ -5.7118 \times 10^{-1} & -7.0984 \times 10^{-1} & -4.1216 \times 10^{-1} & 1.0 & 0.0 \\ -5.0147 \times 10^{-1} & -2.9867 \times 10^{-1} & -8.1199 \times 10^{-1} & 1.0 & 0.0 \\ -3.8672 \times 10^{-1} & 6.9339 \times 10^{-1} & -6.0800 \times 10^{-1} & 1.0 & 0.0 \\ -3.3759 \times 10^{-1} & 3.5243 \times 10^{-1} & -8.7283 \times 10^{-1} & 0.0 & 1.0 \\ 5.9029 \times 10^{-1} & 3.4358 \times 10^{-1} & -7.3042 \times 10^{-1} & 0.0 & 1.0 \\ 1.6708 \times 10^{-1} & 3.8715 \times 10^{-1} & -9.0675 \times 10^{-1} & 0.0 & 1.0 \\ -6.4008 \times 10^{-1} & 2.9773 \times 10^{-1} & -7.0828 \times 10^{-1} & 0.0 & 1.0 \\ 8.7910 \times 10^{-1} & 2.0743 \times 10^{-1} & -4.2913 \times 10^{-1} & 0.0 & 1.0 \\ 9.0053 \times 10^{-2} & 4.7952 \times 10^{-1} & -8.7290 \times 10^{-1} & 0.0 & 1.0 \\ 1.3906 \times 10^{-1} & -4.3905 \times 10^{-1} & -8.8764 \times 10^{-1} & 0.0 & 1.0 \\ -2.4136 \times 10^{-1} & 8.7690 \times 10^{-1} & -4.1568 \times 10^{-1} & 0.0 & 1.0 \\ 3.0684 \times 10^{-1} & 1.0696 \times 10^{-1} & -9.4573 \times 10^{-1} & 0.0 & 1.0 \\ 5.3570 \times 10^{-1} & -2.8382 \times 10^{-1} & -7.9528 \times 10^{-1} & 0.0 & 1.0 \\ -2.6773 \times 10^{-1} & 5.3405 \times 10^{-1} & -8.0194 \times 10^{-1} & 0.0 & 1.0 \\ 1.1111 \times 10^{-1} & 9.6186 \times 10^{-1} & -2.4997 \times 10^{-1} & 0.0 & 1.0 \end{bmatrix}. \quad (4.10)$$

The geometry matrix for satellite geometry 5 is

$$\mathbf{G}_{five} = \left[\begin{array}{cccccc}
8.5334 \times 10^{-1} & -2.1582 \times 10^{-3} & -5.1807 \times 10^{-1} & 1.0 & 0.0 & 0.0 \\
3.7866 \times 10^{-1} & 8.6053 \times 10^{-1} & -3.4119 \times 10^{-1} & 1.0 & 0.0 & 0.0 \\
-2.1614 \times 10^{-1} & 3.9521 \times 10^{-1} & -8.9280 \times 10^{-1} & 1.0 & 0.0 & 0.0 \\
3.5034 \times 10^{-1} & -1.7313 \times 10^{-1} & -9.2048 \times 10^{-1} & 1.0 & 0.0 & 0.0 \\
-9.0776 \times 10^{-1} & 1.5131 \times 10^{-1} & -3.9125 \times 10^{-1} & 1.0 & 0.0 & 0.0 \\
7.7386 \times 10^{-1} & 3.4472 \times 10^{-1} & -5.3134 \times 10^{-1} & 1.0 & 0.0 & 0.0 \\
5.4021 \times 10^{-1} & -6.0939 \times 10^{-1} & -5.8037 \times 10^{-1} & 1.0 & 0.0 & 0.0 \\
-3.0590 \times 10^{-3} & -4.3559 \times 10^{-1} & -9.0014 \times 10^{-1} & 1.0 & 0.0 & 0.0 \\
7.6416 \times 10^{-2} & 6.4019 \times 10^{-1} & -7.6441 \times 10^{-1} & 1.0 & 0.0 & 0.0 \\
-5.7118 \times 10^{-1} & -7.0984 \times 10^{-1} & -4.1216 \times 10^{-1} & 1.0 & 0.0 & 0.0 \\
-5.0147 \times 10^{-1} & -2.9867 \times 10^{-1} & -8.1199 \times 10^{-1} & 1.0 & 0.0 & 0.0 \\
-3.8672 \times 10^{-1} & 6.9339 \times 10^{-1} & -6.0800 \times 10^{-1} & 1.0 & 0.0 & 0.0 \\
2.5858 \times 10^{-1} & 6.8390 \times 10^{-1} & -6.8222 \times 10^{-1} & 0.0 & 1.0 & 0.0 \\
-6.6621 \times 10^{-1} & -5.2417 \times 10^{-1} & -5.3049 \times 10^{-1} & 0.0 & 1.0 & 0.0 \\
-9.9014 \times 10^{-2} & -6.7353 \times 10^{-1} & -7.3250 \times 10^{-1} & 0.0 & 1.0 & 0.0 \\
7.3723 \times 10^{-1} & -4.2378 \times 10^{-1} & -5.2622 \times 10^{-1} & 0.0 & 1.0 & 0.0 \\
-6.1703 \times 10^{-1} & 1.1442 \times 10^{-1} & -7.7858 \times 10^{-1} & 0.0 & 1.0 & 0.0 \\
-3.0099 \times 10^{-1} & 7.5154 \times 10^{-1} & -5.8702 \times 10^{-1} & 0.0 & 1.0 & 0.0 \\
-6.0027 \times 10^{-1} & -5.7338 \times 10^{-1} & -5.5759 \times 10^{-1} & 0.0 & 1.0 & 0.0 \\
-3.3759 \times 10^{-1} & 3.5243 \times 10^{-1} & -8.7283 \times 10^{-1} & 0.0 & 0.0 & 1.0 \\
5.9029 \times 10^{-1} & 3.4358 \times 10^{-1} & -7.3042 \times 10^{-1} & 0.0 & 0.0 & 1.0 \\
1.6708 \times 10^{-1} & 3.8715 \times 10^{-1} & -9.0675 \times 10^{-1} & 0.0 & 0.0 & 1.0 \\
-6.4008 \times 10^{-1} & 2.9773 \times 10^{-1} & -7.0828 \times 10^{-1} & 0.0 & 0.0 & 1.0 \\
8.7910 \times 10^{-1} & 2.0743 \times 10^{-1} & -4.2913 \times 10^{-1} & 0.0 & 0.0 & 1.0 \\
9.0053 \times 10^{-2} & 4.7952 \times 10^{-1} & -8.7290 \times 10^{-1} & 0.0 & 0.0 & 1.0 \\
1.3906 \times 10^{-1} & -4.3905 \times 10^{-1} & -8.8764 \times 10^{-1} & 0.0 & 0.0 & 1.0 \\
-2.4136 \times 10^{-1} & 8.7690 \times 10^{-1} & -4.1568 \times 10^{-1} & 0.0 & 0.0 & 1.0 \\
3.0684 \times 10^{-1} & 1.0696 \times 10^{-1} & -9.4573 \times 10^{-1} & 0.0 & 0.0 & 1.0 \\
5.3570 \times 10^{-1} & -2.8382 \times 10^{-1} & -7.9528 \times 10^{-1} & 0.0 & 0.0 & 1.0 \\
-2.6773 \times 10^{-1} & 5.3405 \times 10^{-1} & -8.0194 \times 10^{-1} & 0.0 & 0.0 & 1.0 \\
1.1111 \times 10^{-1} & 9.6186 \times 10^{-1} & -2.4997 \times 10^{-1} & 0.0 & 0.0 & 1.0
\end{array}\right]. \tag{4.11}$$

4.1 Example 1

The performance of the PQP method is evaluated with three different sets of simulations and the results are presented in this section. In all of the simulations, the components of $\boldsymbol{\epsilon}_n$ are simulated as the independent and identically distributed normal random variables, each of which has mean 0 meters and standard deviation 1 meter. In the first and second sets of simulations, $\mathbf{f}_r$, is simulated by first assuming a maximum number of possible nonzero components. Then a compatible support of $\mathbf{f}_r$ is selected. The nonzero components of $\mathbf{f}_r$ are then modeled by the independent and identically distributed normal random variables, each of which has mean 25 meters and standard deviation 1 meter. All the measurements are weighted equally and $\mathbf{W}$ is the identity matrix of the appropriate dimensions. In addition, the parameter of the PQP is tuned using the bounding the probability of false alarms method. In other words, the parameter is tuned according to (3.27).

4.1.1 Test Case I

In the first test case of the first example, the PQP method, the exhaustive search method, and the Linear Program (LP) formulation of the l_1-minimization method proposed in [92] are compared in terms of computation time. The test satellite geometry is the satellite geometry 5, which consists of 12 GPS, 7 GLONASS, and 12 Beidou satellites. For all the methods, $P_{FA,REQ}$ is set to 1.0×10^{-6} while $P_{C,REQ}$ is set to 2.0×10^{-6}. $P(H_0)$ is set to 9.95×10^{-1}, and $P(H_i)$, as well as P_{max}, is assumed to be 1.0×10^{-5}. The results for all the methods are summarized in Table 4.5. From Table 4.5, the computation time of the PQP method remains to be a few milliseconds and the LP formulation formulation computation time remains to be approximately one millisecond, as n_{fault} increases. The computation time of the exhaustive search method, however, increases exponentially as n_{fault} grows. For the tested satellite geometry with a total number of 31 satellites, the exhaustive search method becomes intractable when n_{fault} grow to be 3 or more.

Table 4.5. The Computation Time of The Three FDE Methods

n_{fault}	computation time (ms)		
	PQP	Exhaustive Search	LP
1	3.563×10^0	5.792×10^1	1.166×10^0
2	3.576×10^0	8.915×10^2	1.175×10^0
3	3.319×10^0	7.154×10^3	9.910×10^{-1}
4	3.383×10^0	4.354×10^4	9.850×10^{-1}
5	3.446×10^0	7.716×10^5	9.580×10^{-1}
6	3.369×10^0	4.449×10^6	1.041×10^0

4.1.2 Test Case II

In the second test case of the first example, the vertical position error of the PQP method is simulated and compared with the results obtained using all of the simulated measurements (No FDE) and the results obtained using only the fault-free subset measurements (Exact FDE). In addition, the results by the exhaustive search method are also included for small n_{fault}. The test satellite geometry is the satellite geometry 5 and the simulation settings are identical to those used the first test case of the first example. For each value of the maximum numbers of possible faults $n_{fault,max}$, 1.0×10^3 simulations are repeated and the vertical position errors are recorded. In each of the simulations, n_{fault} is selected, with equal probability, to be one of the possible numbers of faults. The possible numbers of faults includes 0 for the fault-free hypothesis. After n_{fault} is determined, the support of the true fault vector $\mathbf{f}_r$ is selected from all of the compatible faulty hypothesis H_i, with equal probability. Thus,

$$P_{max} = \frac{1}{31(n_{fault,max} + 1)}. \tag{4.12}$$

The results for the simulations are summarized in Table 4.6. Despite the fact that the exhaustive search method is able to reduce the standard deviation of the vertical position error close to that obtained by the exact FDE, the computation time is too

Table 4.6. Simulation Results: Vertical Position Errors - 1

standard deviation (m)				
n_{fault}	No FDE	Exact FDE	PQP	Exhaustive Search
1	1.950×10^{0}	9.809×10^{-1}	1.005×10^{0}	9.808×10^{-1}
2	2.546×10^{0}	9.817×10^{-1}	1.004×10^{0}	9.818×10^{-1}
3	5.458×10^{0}	1.011×10^{0}	1.073×10^{0}	-
4	6.361×10^{0}	1.019×10^{0}	1.086×10^{0}	-
5	6.692×10^{0}	1.022×10^{0}	1.098×10^{0}	-
6	7.308×10^{0}	1.041×10^{0}	1.113×10^{0}	-
7	7.907×10^{0}	1.068×10^{0}	1.135×10^{0}	-
8	8.168×10^{0}	1.070×10^{0}	1.131×10^{0}	-
9	8.537×10^{0}	1.059×10^{0}	1.134×10^{0}	-

long and it makes the exhaustive search method not practical for $n_{fault,max}$ greater than 2. On the other hand, the PQP method is able to provide reduction in the standard deviation without long computation time.

Also included in the second test case of the first example is a comparison of the vertical position error of the PQP method and that of the LP formulation of the l_1-minimization method proposed in [92]. The results are presented in Table 4.7. For each value of the maximum numbers of possible faults $n_{fault,max}$, 1.0×10^5 simulations are repeated and the vertical position errors are recorded. The LP formulation shows better performance in terms of the vertical position error. Such results agree with the simulation results reported in [92], which shows that the LP formulation is comparable to the exhaustive search method in terms of vertical positioning performance. While being fast and having good performance in terms of vertical positioning error, the integrity risk bound of the LP formulation remains to be an open challenge. Compared to the LP formulation, the PQP method addresses the integrity by the calculation of the integrity risk bound.

Table 4.7. Simulation Results: Vertical Position Errors - 2

standard deviation (m)					
n_{fault}	PQP	LP	n_{fault}	PQP	LP
1	1.025×10^{0}	6.131×10^{-1}	5	1.098×10^{0}	6.684×10^{-1}
2	1.049×10^{0}	6.250×10^{-1}	6	1.103×10^{0}	6.914×10^{-1}
3	1.071×10^{0}	6.429×10^{-1}	7	1.116×10^{0}	7.053×10^{-1}
4	1.082×10^{0}	6.640×10^{-1}			

Table 4.8. Simulation Results: Integrity Risk Bounds

n_{sv}	VDOP	Integrity Risk Bound	n_{sv}	VDOP	Integrity Risk Bound
26	1.215	1.319×10^{-2}	29	1.062	3.727×10^{-4}
26	1.207	1.163×10^{-2}	29	1.056	4.175×10^{-4}
26	1.203	1.101×10^{-2}	29	1.029	2.587×10^{-4}
27	1.138	2.815×10^{-3}	30	1.001	2.880×10^{-4}
27	1.131	2.391×10^{-3}	30	0.994	2.450×10^{-4}
27	1.118	1.675×10^{-3}	30	0.988	2.009×10^{-4}
28	1.101	9.883×10^{-4}	31	0.983	1.529×10^{-5}
28	1.098	8.808×10^{-4}	31	0.979	1.088×10^{-5}
28	1.092	7.021×10^{-4}	31	0.976	8.015×10^{-6}

4.1.3 Test Case III

In the third test case of the first example, the integrity risk bounds are calculated for the test satellite geometries. The simulation settings are identical to those used in the first and the second test cases, and the alarm limit l_{AL} is set to be 30 meters. The hypotheses considered include the fault-free hypothesis, all the one-fault hypotheses, and all the two-fault hypotheses. The calculated integrity risk bounds are summarized in Table 4.8. The calculated integrity bounds show a general trend of decreasing with an increase in the number of measurements n_{sv}. The numbers of measurements for the test geometries used in the third set of simulations range from 26 to 31, which are relatively small or moderate numbers of measurements, when compared to what

Table 4.9. Parameters for Test Case IV

$P_{IR,REQ}$	9.8×10^{-8}
P_{H_i} (one-fault)	1.0×10^{-4}
P_{H_i} (two-fault)	1.0×10^{-8}
P_{FA}	4.0×10^{-6}

are available now and will be in the future. Lower integrity risk bounds are expected when more GNSS measurements are included.

4.2 Example 2

In this second example, test cases are presented for $l_{PL,LB}$ and $l_{PL,UB}$ in the case of detection.

4.2.1 Test Case I

In the first test case of the second example, $l_{PL,LB}$ and $l_{PL,UB}$ are calculated for the satellite geometries summarized in Table 4.4. The parameters used is summarized in Table 4.9.

For all the satellite geometries, $P_{IR,REQ}$ is set to be 9.8×10^{-8}. Also, P_{H_i} is set to be 1.0×10^{-4} for all the one-fault hypotheses and 1.0×10^{-8} for all the two-fault hypotheses. The false alarm probability P_{FA} is set to be 4.0×10^{-6}. The calculated $l_{PL,LB}$ and $l_{PL,UB}$ for the satellite geometries are shown in Table 4.10.

In Table 4.10, both the $l_{PL,LB}$ and $l_{PL,UB}$ show trends of decreasing with increases in number of measurements. Therefore, it suggests that increasing the number of GNSS measurements improves the integrity performance. The vertical alert limits for the Approach with Vertical Guidance-I (APV-I), the Approach with Vertical Guidance-II (APV-II), and the Category I precision approach [5] are summarized in Table 4.11.

Table 4.10. $l_{PL,LB}$ and $l_{PL,UB}$ Calculated Using h

Satellite Geometry	n_{sv}	n_c	h	$l_{PL,LB}$ (m)	$l_{PL,UB}$ (m)
1	8	1	5.5164	66.9641	71.5893
2	12	1	6.2835	40.2435	40.2435
3	19	2	7.1480	34.2639	35.7778
4	24	2	7.7401	32.9910	32.9988
5	31	3	8.3598	30.5461	32.7683

Table 4.11. Vertical Alert Limits for Different Types of Approaches [5]

Type of Approach	Vertical Alert Limit (m)
APV-I	50
APV-II	20
Category I precision approach	$35 - 10$

For all three types of approaches, the required integrity is $1 - 2 \times 10^{-7}$ in any approach and the required continuity is $1-8\times10^{-6}$ per 15 seconds. Except for satellite geometry 1, the results show that the PQP method is worthy of further studies to support fault detection for vertical guidance in the APV-I and the Category I precision approach. For all the satellite geometries, the calculated $l_{PL,LB}$ suggests that the PQP method may not be used for fault detection for vertical guidance in APV-II. The values of the parameter h in Table 4.10 are determined using the bounding the probability of false alarms method. That is, h is tuned according to (3.27). Ideally, h should be determined using

$$h = CDF^{-1}(1 - P_{FA,REQ}), \tag{4.13}$$

where $CDF^{-1}(1-P_{FA,REQ})$ is the inverse cumulative distribution function of $\|Q^T p\|_\infty$, evaluated at $1 - P_{FA,REQ}$ under the faulty-frees hypothesis. However, it is not clear

Table 4.12. $l_{PL,LB}$ and $l_{PL,UB}$ Calculated Using h_{KDE}

Satellite Geometry	n_{sv}	n_c	h_{KDE}	$l_{PL,LB}$ (m)	$l_{PL,UB}$ (m)
1	8	1	3.5711	44.0581	49.4812
2	12	1	3.8631	24.4915	24.4919
3	19	2	4.0112	20.0656	23.1093
4	24	2	4.2510	18.2951	18.9668
5	31	3	4.3145	17.0422	19.0148

how $\|Q^T p\|_\infty$ distributes analytically. As a result, (3.27) is used to tune h [52]. However, the values of h determined using (3.27) are relatively conservative.

4.2.2 Test Case II

In the second test case of the second example, the values of h tuned using the kernel density estimation method. In other words, the values of h are determined using estimations of the cumulative distribution function, which is generated by the simulated samples of $\|Q^T p\|_\infty$. To be more specific, 10000 samples of $\|Q^T p\|_\infty$ are simulated for each of the satellite geometries. Then estimates of the cumulative distribution function, which are obtained using kernel density estimation with the normal kernel smoothing functions [44]. The resulting values of h, denoted as h_{KDE}, and the $l_{PL,LB}$ and the $l_{PL,UB}$ are summarized in Table 4.12.

The $l_{PL,LB}$ and the $l_{PL,UB}$ in Table 4.12 show significant improvement compared to those shown in Table 4.10. Lower and thus more practical $l_{PL,LB}$ and $l_{PL,UB}$ are to be expected if the cumulative distribution function of $\|Q^T p\|_\infty$ can be accurately estimated.

Table 4.13. Simulation Results: Vertical Position Errors - 3

$n_{fault,max}$	standard deviation (m)			
	No FDE	Exact FDE	$h = 8.3598$	$h_{KDE} = 4.3145$
1	3.2885×10^{0}	9.8634×10^{-1}	1.0031×10^{0}	1.0031×10^{0}
2	4.4747×10^{0}	9.9638×10^{-1}	1.0279×10^{0}	1.0279×10^{0}
3	5.3852×10^{0}	1.0073×10^{0}	1.0522×10^{0}	1.0522×10^{0}
4	6.1143×10^{0}	1.0179×10^{0}	1.0769×10^{0}	1.0769×10^{0}
5	6.7638×10^{0}	1.0289×10^{0}	1.0997×10^{0}	1.0997×10^{0}
6	7.3559×10^{0}	1.0429×10^{0}	1.1287×10^{0}	1.1287×10^{0}
7	7.8401×10^{0}	1.0528×10^{0}	1.1621×10^{0}	1.1621×10^{0}
8	8.2698×10^{0}	1.0677×10^{0}	1.2214×10^{0}	1.2214×10^{0}

4.2.3 Test Case III

In the third test case of the second example, the standard deviation of the vertical position error resulting from h_{KDE} is studied using the satellite geometry 5 in Table 4.4. One million simulations were conducted for each $n_{fault,max}$ in Table 4.13.

In Table 4.13, $n_{fault,max}$ is the number of maximum faulty measurements. For example, if $n_{fault,max}$ is 2, then it means that the measurements may be fault-free, may contain one faulty measurement, or may contain two faulty measurements. For each $n_{fault,max}$, the number of faulty measurements is determined using the prior probabilities described below. The prior probability that all measurements are fault-free is set to be

$$P_0 = \frac{1}{n_{fault,max} + 1}, \tag{4.14}$$

and the prior probability that n_{fault} measurements are faulty is set to be

$$P_{n_{fault}} = \frac{1 - P_0}{n_{fault,max}}. \tag{4.15}$$

The fault hypothesis imposed in each simulation is selected with equal probability after the number of faulty measurements, n_{fault}, is determined. To be specific, the

Table 4.14. Parameters for Test Case III

$P_{C,REQ}$	2.0×10^{-6}
P_{FA}	1.0×10^{-6}
$P(H_0)$	$\frac{1}{n_{fault,max}+1}$
P_{max}	$\frac{1}{31(n_{fault,max}+1)}$

Table 4.15. Noise Parameters

	mean	standard deviation
ϵ_n	0 meters	1 meter
f_r	0 meters	25 meters

fault hypothesis is selected with equal probability from all the fault hypotheses that have exactly n_{fault} faulty measurements. The parameters related to the threshold calculations are summarized in Table 4.14. In this test case, ϵ_n is modeled as a normal random vector whose components are independent and each has 0 meters mean and 1 meter standard deviation. Also f_r is modeled as a normal random vector whose components are independent and each has 0 meters mean and 25 meters standard deviation. These values are summarized in Table 4.15. The values in the No FDE column are the standard deviations of the vertical position error resulting from all the measurements and the values in the Exact FDE column are those resulting from the fault-free measurements only, while the values in the h and h_{KDE} columns are those resulting from the PQP method with the corresponding values of the PQP parameter. From Table 4.13, the standard deviations of the vertical position error, which are resulting from h_{KDE}, are almost identical to those from h. This is because the same measurements have been excluded for both h and h_{KDE} in most of the simulations. For the purpose of illustration, the PQP method is applied to satellite geometry 5 with different values of the PQP parameter. Starting from 1, the PQP

Table 4.16. Different PQP Parameters and the Exclusion

PQP Parameter	Measurements Excluded
1.00	4,5,6,8,11,12,15,18,26,27,29,30,31
1.25	4,5,6,11,12,15,18,26,27,29,30,31
1.50	4,5,6,11,12,15,18,27,29,30,31
1.75	4,5,6,11,12,18,27,29,31
3.00	4,5,11,12,18,27,29,31
8.50	4,5,11,12,18,29,31
9.50	4,5,11,12,18,27,29,31
11.50	4,5,11,12,18,29,31

Table 4.17. Parameters for Test Case IV

number of faulty measurements	5
value of each nonzero components	20 meters

method is applied and the set of measurements excluded by the PQP method is recorded. The PQP method is then repeated with a 0.25 increment in the PQP parameter, while $\boldsymbol{\epsilon}_n$ and $\mathbf{f}_r$ remain unchanged. The set of excluded measurements is recorded if it is different from the one in the previous iteration. The results are shown in Table 4.16.

From Table 4.16, the set of measurements excluded remains unchanged for the PQP parameter ranging from 3.00 to 8.25. Therefore, using h_{KDE} instead of h as the PQP parameter has a very limited impact on the vertical positioning accuracy. At the same time, comparing Table 4.12 and Table 4.10 suggests that the use of h_{KDE} leads to great reductions in vertical protection level.

4.2.4 Test Case IV

In the fourth test case of the second example, the use of the PQP method to estimate the number of faulty measurements is demonstrated. The setting is identical to the previous test case of the second example except for that the nonzero components of the fault vector now have constant values. In order to obtain an estimate of the number of the faulty measurements, the PQP is first solved with a small h. If the result of the PQP method is no detection, then there is no faulty measurement. If the result of the PQP method is exclusion, then the value of h is increased and the PQP is solved again with the new h, whose value has been increased. The number of the nonzero components of the solution is recorded. The process of increasing the value of h and solving the PQP is repeated until the result of the PQP is detection. To illustrate the process, simulations are conducted with 5 faulty measurements, and the values of the nonzero components of the fault vector are set to be 20 meters. These values are summarized in Table 4.17. The results are shown in Table 4.18.

From the results in Table 4.18, the estimated number of faulty measurements is 5, which is the number of candidates of faulty measurements when the value of h ranges from 2.75 to 13.25. The idea behind this estimation of the number of faulty measurements is that increasing the value of h generally reduces the number of the nonzero components of the solution to the PQP, which is reported in [39]. Under the assumption that the received measurements are not fault-free, increasing the value of h eventually results in one or more faulty measurements not associated with the nonzero components of the solution to the PQP, which in turn lead to failure of passing the RAIM test in Figure 3.1. The magnitude of the nonzero components that are not associated with the nonzero components of the solution to the PQP consequently affect the quality of the estimate of the number of faulty measurements. It suffices to lead to the result of detection in Figure 3.1 if there is a faulty measurement associated with any of the nonzero components of the PQP solution and the magnitude of the corresponding component of the fault vector is large. In this case, the estimate of the number of faulty measurements is more accurate. However, it may take two or more faulty measurements with smaller magnitudes of the corresponding components

Table 4.18. Estimating the Number of Faulty Measurements

PQP Parameter	Candidates of Faulty Measurements
1.00	1,2,3,4,7,8,12,19,21,22,28,31
1.25	1,2,3,4,7,8,12,19,21,22,28
1.50	1,2,3,4,7,8,19,21,22
1.75	1,2,3,4,7,19
2.00	1,2,3,4,19
2.25	1,2,3,4,7,19
2.75	1,2,3,4,19
13.50	detection claimed

Table 4.19. The Effect of the Magnitudes of the Nonzero Fault Vector Components (An Example with 5 Faulty Measurements)

Magnitude of the Nonzero Fault Vector Components (m)	Estimated Number of Faulty Measurements
50.00	5
25.00	5
20.00	5
15.00	5
10.00	5
5.00	2
2.50	1

of the fault vector to lead to the result of detection in Figure 3.1, and the estimated number of faulty measurements is therefore less than the actual number of faulty measurements. Table 4.19 demonstrates this effect of the magnitudes of the nonzero components of fault vector.

5. SUMMARY

The use of the multi-constellation GNSS offers performance improvements but also poses new challenges in safety-critical applications, which include civil aviation. The increased numbers of measurements provide not only better satellite geometries but also better redundancy for considerations beyond positioning accuracy. In this work, the redundancy is considered for vertical navigation of aircraft through the PQP method that detects and excludes faulty GNSS measurements and the integration of the PQP method with the integrity risk and the continuity risk bounds for fault detection and exclusion using the ARAIM. The PQP method is able to detect and exclude faulty measurements in a computationally efficient fashion, and the integration of the PQP method with the integrity risk and the continuity risk moves the PQP method forward to the goal of integrity monitoring for vertical navigation, despite the calculation of the integrity risk bound is still combinatorial. The integration of the PQP method with the continuity risk bound allows for a way to tune the parameter for the PQP approach according to the requirements on false alarm probability, and integration of the PQP approach with the integrity risk bound facilitates the determination of fulfillment of integrity requirement, both of which are necessary for evaluating the PQP approach for safety-critical applications. With the test satellite geometries, the first numerical example and the test cases show that the PQP approach is fast and effective in improving vertical positioning accuracy. Also, the calculated integrity risk bounds show a general decreasing trend with an increasing number of measurements. However, the numerical values of preliminary simulation results also suggest that improvements should be made to tighten the integrity risk bound for the PQP approach. It is emphasized that while detection and exclusion of faulty GNSS measurements with the PQP approach avoids exhaustive search, but the calculation of integrity risk bound is still combinatorial. Consequently, the PQP

approach is not a practical integrity monitoring method despite it is able to detect and exclude faulty measurements in a computationally efficient fashion. Nevertheless, improvements to reduce the computational load of the integrity risk bound calculation for the Chi-squared RAIM fault detection and exclusion can be applied readily to the integrity risk bound calculation PQP approach. Moreover, further researches on the PQP parameter tuning methods can be pursued to tighten the current integrity bound for the PQP approach.

In addition to the integrity risk bound, the vertical protection level calculation for the PQP approach is formulated. Integrated with the vertical protection level calculation of the solution separation ARAIM, similar vertical protection level and the associated upper and lower bounds are formulated for the fault detection using the PQP approach. The second numerical example and the test cases which consists of GPS, GLONASS, and Beidou measurements show that, in general, increasing the number of measurements reduces the calculated upper and lower bounds of vertical protection level. Also, the results suggest that it may be possible to use the PQP approach for fault detection for the vertical navigation of aircraft in the APV-I and the category I precision approach.

Furthermore, there is still room for further enhancement of the integrity performance for fault detection and exclusion with the PQP approach. One direction for the enhancement is related to the estimation of the cumulative distribution function of $\|Q^T p\|_\infty$. If the cumulative distribution function can be accurately estimated, then h can be determined using the estimated cumulative distribution function and reductions in $l_{PL,LB}$ and $l_{PL,UB}$ will result. Lower and more practical l_{PL} can therefore be obtained. The application of extreme value theory and the conservative estimation of the tail probability are believed to be the key elements of further researches in this direction [76, 93, 94]. In addition, the connection between the PQP approach and the SVM may shed light upon researches related to the parameter tuning for the PQP approach.

Another direction for the enhancement is to find more efficient methods to solve the vertical protection level for the detection and exclusion of faulty GNSS measurements using the PQP approach. To be more precise, more efficient numerical methods and algorithms should be sought and carefully studied to solve the problem described by (3.126), (3.127), (3.128), and (3.129).

REFERENCES

[1] *FAA needs to implement more efficient performance-based navigation procedures and clarify the role of third parties.* U.S. Dept. of Transportation, Office of the Secretary of Transportation, Office of Inspector General, Washington, D.C., 2010.

[2] ICAO Doc. 9613. *Performance Based Navigation (PBN) Manual*, 4 edition, 2013.

[3] Federal Aviation Administration overview on PBN. `https://www.icao.int/APAC/APAC-RSO/PBN%20Workshop%20for%20Air%20Traffic%20Controllers/FAA%20Overview%20on%20PBN.pdf`.

[4] US Federal Aviation Administration. *GLOBAL POSITIONING SYSTEM WIDE AREA AUGMENTATION SYSTEM (WAAS) PERFORMANCE STANDARD*, 2008.

[5] Richard Farnworth. Aviation applications. In Peter J. G. Teunissen and Oliver Montenbruck, editors, *Springer Handbook of Global Navigation Satellite Systems*, chapter 30, pages 877–904. Springer International Publishing, 2017.

[6] *Instrument flying handbook.* U.S. Dept. of Transportation, Federal Aviation Administration, Flight Standards Service :–For sale by the Supt. of Docs., U.S. G.P.O.,, 2012.

[7] Christopher Hegarty. The global positioning system (GPS). In Peter J. G. Teunissen and Oliver Montenbruck, editors, *Springer Handbook of Global Navigation Satellite Systems*, chapter 7, pages 197–218. Springer International Publishing, 2017.

[8] Yuanxi Yang, Jing. Tang, and Oliver. Montenbruck. Chinese navigation satellite systems. In Peter J. G. Teunissen and Oliver Montenbruck, editors, *Springer Handbook of Global Navigation Satellite Systems*, chapter 10, pages 273–304. Springer International Publishing, 2017.

[9] M. Falcone, J. Hahn, and T. Burger. Galileo. In P. J. G. Teunissen and O. Montenbruck, editors, *Springer Handbook of Global Navigation Satellite Systems*, chapter 9, pages 247–272. Springer International Publishing, 2017.

[10] Sergey Revnivykh, Alexey Bolkunov, Alexander Serdyukov, and Oliver Montenbruck. GLONASS. In Peter J. G. Teunissen and Oliver Montenbruck, editors, *Springer Handbook of Global Navigation Satellite Systems*, chapter 8, pages 219–246. Springer International Publishing, 2017.

[11] John W. Betz. *Satellite-based Navigation and Timing : Engineering Systems, Signals, and Receivers.* Wiley-IEEE Press, 2008.

[12] Todd Walter. Satellite based augmentation systems. In Peter J. G. Teunissen and Oliver Montenbruck, editors, *Springer Handbook of Global Navigation Satellite Systems*, chapter 12, pages 339–362. Springer International Publishing, 2017.

[13] Samuel Pullen. Ground based augmentation systems. In Peter J. G. Teunissen and Oliver Montenbruck, editors, *Springer Handbook of Global Navigation Satellite Systems*, chapter 31, pages 905–932. Springer International Publishing, 2017.

[14] Christopher J. Hegarty, Joe. Leva, Karen Van Dyke, and Todd Walter. Performance of stand-alone gnss. In Elliott D. Kaplan and Christopher J. Hegarty, editors, *Understanding GPS/GNSS : principles and applications*, chapter 11, pages 661–707. Artech House, third edition. edition, 2017.

[15] Per K. Enge and A. J. Van Dierendonck. Wide area augmentation system. In Bradford W. Parkinson, Per Enge, Penina Axelrad, and James J. Spilker Jr., editors, *Global Positioning System: Theory and Applications, Volume II*, chapter 30, pages 117–142. American Institute of Aeronautics and Astronautics, 1996.

[16] Bill Wanner, Bruce Decleene, David A. Nelthropp, and Stephen Gordon. Wide area augmentation system vertical accuracy assessment in support of lpv200 requirements. *Navigation*, 55(3):191–203, 2008.

[17] T. Sakai and H. Tashiro. MSAS status. In *26th International Technical Meeting of the Satellite Division of the Institute of Navigation, ION GNSS 2013*, volume 3, pages 2343–2360. Institute of Navigation, 2013.

[18] Javier Ventura-TravesetJ, Carlos Lopez de Echazarreta, Juan-Pedro Lam, and Didier Flament. An introduction to EGNOS: The european geostationarynavigation overlay system. In Jari Nurm and Stephan Sand, editors, *GALILEO Positioning Technology*, Signals and Communication Technology, chapter 14, pages 323–358. Springer, 2015.

[19] K N Suryanarayana Rao. Gagan - the indian satellite based augmentation system. *Indian Journal of Radio and Space Physics*, 36(4):293–302, 2007.

[20] Sergey Karutin. SDCM program status. In *25th International Technical Meeting of the Satellite Division of the Institute of Navigation 2012, ION GNSS 2012*, volume 2, pages 1034–1044, 2012.

[21] Yuanxi Yang, Weiguang Gao, Shuren Guo, Yue Mao, and Yufei Yang. Introduction to beidou-3 navigation satellite system. *Navigation*, 66(1):7–18, 2019.

[22] Dong-geun. Han, Ho Hyun Yun, O. Kim, Chae-Soo. Kim, and C. Kee. Korean SBAS development progress and test results of pseudolite-based demo system. In *Institute of Navigation International Technical Meeting 2014, ITM 2014*, pages 219–222. Institute of Navigation, 2014.

[23] Bradford W. Parkinson and Penina Axelrad. Autonomous gps integrity monitoring using the pseudorange residual. *Navigation*, 35(2):255–274, 1988.

[24] R. Grover Brown. Receiver autonomous integrity monitoring. In Bradford W. Parkinson, Per Enge, Penina Axelrad, and James J. Spilker Jr., editors, *Global Positioning System: Theory and Applications, Volume II*, chapter 30, pages 143–166. American Institute of Aeronautics and Astronautics, 1996.

[25] Pratap Misra. Integrated use of gps and glonass in civil aviation. *The Lincoln Laboratory Journal*, 6(2):231–248, 1993.

[26] Juan. Blanch, Todd. Walter, Per. Enge, S. Wallner, F.A. Fernandez, R. Dellago, R. Ioannides, B. Pervan, I.F. Hernandez, B. Belabbas, A. Spletter, and M. Rippl. A proposal for multi-constellation advanced raim for vertical guidance. In *24th International Technical Meeting of the Satellite Division of the Institute of Navigation 2011, ION GNSS 2011*, volume 4, pages 2665–2680, 2011.

[27] Todd Humphreys. Inference. In Peter J. G. Teunissen and Oliver Montenbruck, editors, *Springer Handbook of Global Navigation Satellite Systems*, chapter 16, pages 469–504. Springer International Publishing, 2017.

[28] Michael S. Braasch. Multipath. In Peter J. G. Teunissen and Oliver Montenbruck, editors, *Springer Handbook of Global Navigation Satellite Systems*, chapter 15, pages 443–468. Springer International Publishing, 2017.

[29] Norbert Jakowski. Ionosphere monitoring. In Peter J. G. Teunissen and Oliver Montenbruck, editors, *Springer Handbook of Global Navigation Satellite Systems*, chapter 39, pages 1139–1162. Springer International Publishing, 2017.

[30] Davide Margaria and Marco Pini. The spoofing menace. In Fabio Dovis, editor, *GNSS interference, threats, and countermeasures*, GNSS technology and applications series, chapter 3, pages 67–87. Artech House, 2015.

[31] Inna Kozlov and Alexander Petukhov. Sparse solutions of underdetermined linear systems. In *Handbook of Geomathematics: Second Edition*, pages 2773–2798. Springer Berlin Heidelberg, 2015.

[32] Andrey Nikolayevich Tikhonov. *Numerical Methods for the Solution of Ill-Posed Problems*. Mathematics and Its Applications ; 328. 1st ed. 1995. edition, 1995.

[33] David L. Donoho and Xiaoming Huo. Uncertainty principles and ideal atomic decomposition. *IEEE Transactions on Information Theory*, 47(7):2845–2862, 2001.

[34] Thomas H. Cormen, Charles E. Leiserson, Ronald L. Rivest, and Clifford Stein. *Introduction to algorithms*. MIT Press, third edition edition, 2009.

[35] Stephane G. Mallat and Zhifeng Zhang. Matching pursuits with time-frequency dictionaries. 41(12), 1993.

[36] Scott Shaobing Chen, David L. Donoho, and Michael A. Saunders. Atomic decomposition by basis pursuit. *SIAM Review*, 43(1):129–159, 2001.

[37] Joel A. Tropp and Anna C. Gilbert. Signal recovery from random measurements via orthogonal matching pursuit. *IEEE Transactions on Information Theory*, 53(12):4655–4666, 2007.

[38] Balas Natarajan. Sparse approximate solutions to linear systems. *SIAM J COMPUT*, 24(2):227–234, 1995.

[39] Jean-Jacques Fuchs. Recovery of exact sparse representations in the presence of bounded noise. *IEEE Transactions on Information Theory*, 51(10):3601–3608, 2005.

[40] Mark A. Davenport, Marco F. Duarte, Yonina C. Eldar, and Gitta Kutyniok. Introduction. In *Compressed sensing theory and applications*. Cambridge University Press, Cambridge ; New York, 2012.

[41] Simon Foucart. *A Mathematical Introduction to Compressive Sensing*. Springer New York : Imprint: Birkhäuser, 1st ed. 2013.. edition, 2013.

[42] Yaakov Tsaig. *Sparse solution of underdetermined linear systems: Algorithms and applications.* PhD thesis, Stanford University, 2007.

[43] Emmanuel J. Candes and Terence Tao. Decoding by linear programming. *IEEE Transactions on Information Theory*, 51(12):4203–4215, 2005.

[44] Adrian W. Bowman and Adelchi Azzalin. *Applied smoothing techniques for data analysis : the kernel approach with S-Plus illustrations*. Clarendon Press ; Oxford University Press, Oxford : New York, 1997.

[45] Shau-Shiun Jan. *AIRCRAFT LANDING USING A MODERNIZED GLOBAL POSITIONING SYSTEM AND THE WIDE AREA AUGMENTATION SYSTEM*. PhD thesis, Stanford University, 2014.

[46] John A. Klobuchar. Design and characteristics of the gps ionospheric time delay algorithm for single frequency users. In *Record - IEEE PLANS, Position Location and Navigation Symposium*, pages 280–286. IEEE, 1986.

[47] Harold D. Black. An easily implemented algorithm for the tropospheric range correction. *Journal of Geophysical Research: Solid Earth*, 83(B4):1825–1828, 1978.

[48] Christopher J. Hegarty, Elliott D. Kaplan, Marrten Uijt de Haag, and Ron Cosentino. Gnss errors. In Elliott D. Kaplan and Christopher J. Hegarty, editors, *Understanding GPS/GNSS : principles and applications*, chapter 10, pages 619–660. Artech House, third edition. edition, 2017.

[49] Sandra Verhagen and Peter J.G. Teunissen. Least-squares estimation and kalman filtering. In Peter J. G. Teunissen and Oliver Montenbruck, editors, *Springer Handbook of Global Navigation Satellite Systems*, chapter 22, pages 639–660. Springer International Publishing, 2017.

[50] Scott Gleason and Demoz Gebre-Egziabher. *GNSS applications and methods*. GNSS technology and applications series. Artech House, Boston, Mass., 2009.

[51] Dennis Odijk. Positioning model. In Peter J. G. Teunissen and Oliver Montenbruck, editors, *Springer Handbook of Global Navigation Satellite Systems*, chapter 21, pages 605–638. Springer International Publishing, 2017.

[52] Teng-Yao Yang and Dengfeng Sun. Global navigation satellite systems fault detection and exclusion: a parameterized quadratic programming approach. *IEEE Transactions on Aerospace and Electronic Systems*, 2019.

[53] Gilbert Strang. *Linear algebra and its applications*. Academic Press, 2nd ed. edition, 1980.

[54] Larry Wasserman. *All of Statistics A Concise Course in Statistical Inference*. 2004.

[55] R. Grover Brown. A baseline gps raim scheme and a note on the equivalence of three raim methods. *Navigation*, 39(3):301–316, 1992.

[56] Young Lee. Analysis of range and position comparison methods as a means to provide gps integrity in the user receiver. In *Institute of Navigation, Annual Meeting, 42nd, Seattle, WA; UNITED STATES; 24-26 June 1986*, pages 1–4, 1986.

[57] Mark A. Sturza. Navigation system integrity monitoring using redundant measurements. *Navigation*, 35(4):483–501, 1988.

[58] Sheldon Axler. *Linear Algebra Done Right*. Undergraduate Texts in Mathematics. Springer International Publishing : Imprint: Springer, 3rd ed. edition, 2015.

[59] Efstratios Gallopoulos. *Parallelism in Matrix Computations*. Springer Netherlands : Imprint: Springer, 1st ed. 2016. edition, 2016.

[60] Arak M Mathai. *Quadratic forms in random variables : theory and applications*. M. Dekker, New York, 1992.

[61] Todd Walter and Per Enge. Weighted raim for precision approach. In *Proceedings of ION GPS*, volume 2, pages 1995–2004, 1995.

[62] Mathieu Joerger and Boris Pervan. Fault detection and exclusion using solution separation and chi-squared araim. *IEEE Transactions on Aerospace and Electronic Systems*, 52(2):726–742, 2016.

[63] David G. Luenberger. *Linear and nonlinear programming David G. Luenberger, Yinyu Ye.* Springer, New York, third edition. edition, 2008.

[64] Jean-Jacques Fuchs. More on sparse representations in arbitrary bases. 36(16):1315–1320, 2003.

[65] Yurii Nesterov and Arkadii Nemirovskii. *Interior-Point Polynomial Algorithms in Convex Programming*. Society for Industrial and Applied Mathematics, 1994.

[66] Stephen Boyd and Lieven Vandenberghe. *Convex optimization*. Cambridge University Press, Cambridge, UK ; New York, 2004.

[67] Marguerite Frank and Philip Wolfe. An algorithm for quadratic programming. *Naval Research Logistics Quarterly*, 3(1-2):95–110, 1956.

[68] Bradford W. Parkinson and Penina Axelrad. *Navigation*, 35(2):255–274.

[69] E. Blum and W. Oettli. Direct proof of the existence theorem for quadratic programming. *Operations Research*, 20(1):165–167, 1972.

[70] Naum Zuselevich Shor. *Minimization Methods for Non-Differentiable Functions*. Springer Series in Computational Mathematics, 3. 1st ed. 1985. edition, 1985.

[71] Roger Fletcher. *Practical Methods of Optimization*. Wiley, Hoboken, 2nd ed. edition, 2013.

[72] Jean-Jacques Fuchs. The generalized likelihood ratio test and the sparse representations approach. volume 6134, pages 245–253, 2010.

[73] Vladimir Vapnik. *The Nature of Statistical Learning Theory*. Information Science and Statistics. Second edition. edition, 2000.

[74] Trevor Hastie, Jerome Friedman, and Robert Tibshirani. *The Elements of Statistical Learning Data Mining, Inference, and Prediction*. Springer Series in Statistics. Springer, 2001.

[75] Federico Girosi. An equivalence between sparse approximation and support vector machines. *Neural Computation*, 10(6):1455–1480, 1998.

[76] Jordan Larson and Demoz Gebre-Egziabher. Conservatism assessment of extreme value theory overbounds. *IEEE Transactions on Aerospace and Electronic Systems*, 53(3):1295–1307, 2017.

[77] Nachman Aronszajn. Theory of reproducing kernels. *Transactions of the American Mathematical Society*, 68(3):337–404, 1950.

[78] Peter J Huber. *Robust statistics*. Wiley series in probability and mathematical statistics. Wiley, New York, 1981.

[79] Arthur E. Frazho. Notes on probability. `https://engineering.purdue.edu/AAECourses/aae567/2016/probability.pdf`, 2016.

[80] John E. Angus. RAIM with multiple faults. *Navigation*, 53(4):249–257, 2006.

[81] Mathieu Joerger and Boris Pervan. Kalman filter-based integrity monitoring against sensor faults. *Journal of Guidance, Control, and Dynamics*, 36(2):349–361, 2013.

[82] Juan Blanch, Todd Walter, Per Enge, Young Lee, Boris Pervan, Markus Rippl, and Alex Spletter. Advanced RAIM user algorithm description: Integrity support message processing, fault detection, exclusion, and protection level calculation. In *Proceedings of the 25th International Technical Meeting of The Satellite Division of the Institute of Navigation*, pages 2828–2849, 2012.

[83] Marvin Zelen and Norman C. Severo. Probability functions handbook of mathematical functions with formulas, graphs, and mathematical tables. chapter 26, pages 925–996. 1972.

[84] James O. Ramsay and Bernard W. Silverman. *Functional Data Analysis*. Springer Series in Statistics. 1997.

[85] Artur Gramacki. *Nonparametric Kernel Density Estimation and Its Computational Aspects*. Studies in Big Data, 37. 1st ed. 2018. edition, 2018.

[86] Teng-Yao Yang and Dengfeng Sun. Vertical protection level for GNSS fault detection using parameterized quadratic programming method. *Submitted to the Journal of Aerospace Information Systems*, 2020.

[87] Qt creator manual 4.5.2. `http://doc.qt.io/qtcreator`. The Qt Company.

[88] Eigen v3. `http://eigen.tuxfamily.org`. Gaël Guennebaud and Benoît Jacob., et al.

[89] Boris Schäling. *The Boost C++ Libraries*. XML Press, 2011.

[90] Arindam Mukherjee. *Learning Boost C++ Libraries*. Packt Publishing, 1st edition edition, 2015.

[91] Gurobi optimizer reference manual. `http://www.gurobi.com`. Gurobi Optimization.

[92] Juan. Blanch, Todd. Walter, and Per. Enge. Fast multiple fault exclusion with a large number of measurements. In *Institute of Navigation International Technical Meeting 2015, ITM 2015*, pages 696–701. Institute of Navigation, 2015.

[93] Paul Embrechts. *Modelling Extremal Events for Insurance and Finance*. Stochastic Modelling and Applied Probability, 33. 1st ed. 1997. edition, 1997.

[94] Stuart Coles. *An Introduction to Statistical Modeling of Extreme Values*. Springer Series in Statistics. 1st ed. 2001. edition, 2001.